Neurobiology of Disease 218 (2026) 107217

Contents lists available at ScienceDirect

Neurobiology of Disease

journal homepage: www.elsevier.com/locate/ynbdi

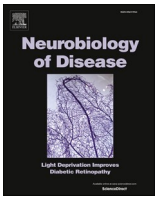

Shank3B$^{-/-}$ pathophysiology: Early metformin treatment rescues behavioural deficits and normalises exacerbated mRNA translation

Laura Marsal-García [a,1], Jung-Hyun Choi [a,b,1], Eve Peraldi [a], Pei You Wu [c], Cong Loc Dang [c], R. Anne McKinney [c], Ilse Gantois [a,*,2], Nahum Sonenberg [a,*,2]

[a] Department of Biochemistry, Goodman Cancer Institute, McGill University, Montreal, Quebec H3A 1A3, Canada
[b] Department of Biochemistry, Chungbuk National University, Cheongju 28644, Republic of Korea
[c] Department of Pharmacology & Therapeutics, McGill University, Montreal, Quebec H3G 0B1, Canada

ARTICLE INFO

Keywords:
Phelan-McDermid syndrome
Shank3 KO mouse model
Metformin
Autism spectrum disorder
Learning and memory
mTORC1
MAPK/ERK

ABSTRACT

Phelan-McDermid syndrome (PMS), a rare neurodevelopmental disorder associated with autism spectrum disorder and intellectual disability, is caused by either deletions in human chromosome 22q13 or mutations in the SH3 and multiple ankyrin repeat domains 3 *(SHANK3)* gene. PMS is highly debilitating, and existing treatments are ineffective. SHANK3 interacts with at least 3 synaptic receptors through synaptic-associated proteins, some of which are upstream of the mammalian/mechanistic target of rapamycin complex 1 (mTORC1) and mitogen-activated protein kinase/extracellular signal-regulated kinase (MAPK/ERK) signalling pathways. Metformin, an inhibitor of the mTORC1 and MAPK/ERK signalling pathways, was shown to correct core phenotypes in a fragile X mouse model, offering therapeutic potential for PMS. Male *Shank3B*$^{-/-}$, a PMS mouse model, and wild-type mice were treated from birth with metformin (5 mg/mL) or vehicle. *Shank3B*$^{-/-}$ mice displayed increased self-grooming, decreased social interaction, reduced duration and frequency of ultrasonic vocalisations, and impaired hippocampal-dependent memory. Upregulated mTORC1 activity was observed in the hippocampus and prefrontal cortex, along with decreased synaptosomal protein expression in the striatum of GluN2B (an *N*-methyl-D-aspartate receptor (NMDAR) subunit), Homer1 (a synaptic-associated protein) and GluA2 (an α-amino-3-hydroxy-5-methyl-4-isoxazolepropionic acid receptor (AMPAR) subunit), all of which interact with Shank3. Metformin treatment from birth corrected core behavioural impairments, exaggerated mRNA translation, and decreased striatal synaptic protein expression. Considering its exceptional safety profile, metformin is a promising therapeutic option for a rapid clinical translation of PMS treatment.

1. Introduction

Phelan-McDermid syndrome (PMS) is a rare neurodevelopmental disorder occurring in approximately one in 10,000 people (Phelan-McDermid Syndrome Foundation, 2025). It is caused by a deletion of the distal portion of chromosome 22q13 or a mutation/deletion of the SH3 and multiple ankyrin repeat domains 3 *(SHANK3)* gene (Phelan et al., 2022). The disease is manifested by developmental delay, speech impairment, and neonatal hypotonia (Cammarata-Scalisi et al., 2022). The majority of children (80 %) display autism spectrum disorder (ASD), and 77 % suffer from moderate to severe intellectual disability (ID) (Cammarata-Scalisi et al., 2022).

ASD is a prevalent neurodevelopmental disorder diagnosed in one in 36 children aged 8 years in the USA, according to the Centers for Disease Control and Prevention, with an incidence rate four times higher in males than in females (Maenner et al., 2023). The core features of ASD are social communication deficits and repetitive behaviour (American Psychiatric Association, 2013). Associated conditions are sleep and mood disorders, anxiety, attention deficit hyperactivity disorder (ADHD), seizures, and ID (American Psychiatric Association, 2013).

* Corresponding authors.
E-mail addresses: laura.marsalgarcia@mail.mcgill.ca (L. Marsal-García), junghyun@cbnu.ac.kr (J.-H. Choi), eve.peraldi@mail.mcgill.ca (E. Peraldi), pei.y.wu@mail.mcgill.ca (P.Y. Wu), cong.l.dang@mail.mcgill.ca (C.L. Dang), anne.mckinney@mcgill.ca (R.A. McKinney), ilse.gantois@mcgill.ca (I. Gantois), nahum.sonenberg@mcgill.ca (N. Sonenberg).
[1] These authors contributed equally to this work.
[2] These authors contributed equally to supervising this work.

https://doi.org/10.1016/j.nbd.2025.107217
Received 30 October 2025; Received in revised form 28 November 2025; Accepted 3 December 2025
Available online 4 December 2025

Memory plays a crucial role in forming social relationships by enriching conversational material with personal memories, thereby rendering interactions reliable and empathic (Bluck, 2003). Impairments in memory exacerbate PMS and ASD symptoms (Desaunay et al., 2020). Memory impairments in PMS patients have been reported as compared to controls and individuals with idiopathic ASD during the post-switch presentation of a visual-comparison task (Guillory et al., 2021).

SHANK3 is a member of the SHANK synaptic scaffolding protein family, which also includes SHANK1 and 2 (Sheng and Kim, 2000). It resides in excitatory synapses and contains five conserved domains (Fig. 1): ankyrin repeat (ANK), Src homology-3 (SH3), postsynaptic density 95/Discs large/Zonula occludens-1 (PDZ), proline-rich (Pro), and sterile-alpha motif (SAM) (Delling and Boeckers, 2021; Sheng and Kim, 2000). The domains interact with actin filaments through α-fodrin and cortactin, and with various receptors through synaptic-associated proteins: Homer, guanylate kinase-associated protein (GKAP), postsynaptic density protein 95 (PSD-95), and glutamate receptor-interacting protein (GRIP), to sustain the function and structure of the synapse (Sheng and Kim, 2000; Urrutia-Ruiz et al., 2022). Some of the receptors are metabotropic glutamate receptors (mGluRs), α-amino-3-hydroxy-5-methyl-4-isoxazolepropionic acid receptors (AMPARs), and *N*-methyl-D-aspartate receptors (NMDARs) upstream of the mammalian/mechanistic target of rapamycin complex 1 (mTORC1) and mitogen-activated protein kinase/extracellular signal-regulated kinase (MAPK/ERK) signalling pathways (Gallagher et al., 2004; Krapivinsky et al., 2003; Santini and Klann, 2014).

SHANK3 plays a key role in synaptic transmission, dendritic spine maturation, cytoskeleton organisation, and hippocampus-dependent learning and memory (Durand et al., 2012; Kouser et al., 2013; Wang et al., 2014). Beyond its well-established postsynaptic role, SHANK3 also influences presynaptic function via Neurexin-Neuroligin trans-synaptic signalling (Arons et al., 2012), underscoring its importance in bidirectional synaptic communication. In addition to its main role in excitatory synapses, recent evidence highlights an important contribution to neuron-oligodendrocyte interactions. SHANK3 is expressed in oligodendrocytes and contributes to their maturation and myelination (Ma et al., 2025), processes that rely on glutamate released from neurons. Proper myelination is essential for neuronal function and axonal conductivity, and SHANK3 deficiency has been associated with white

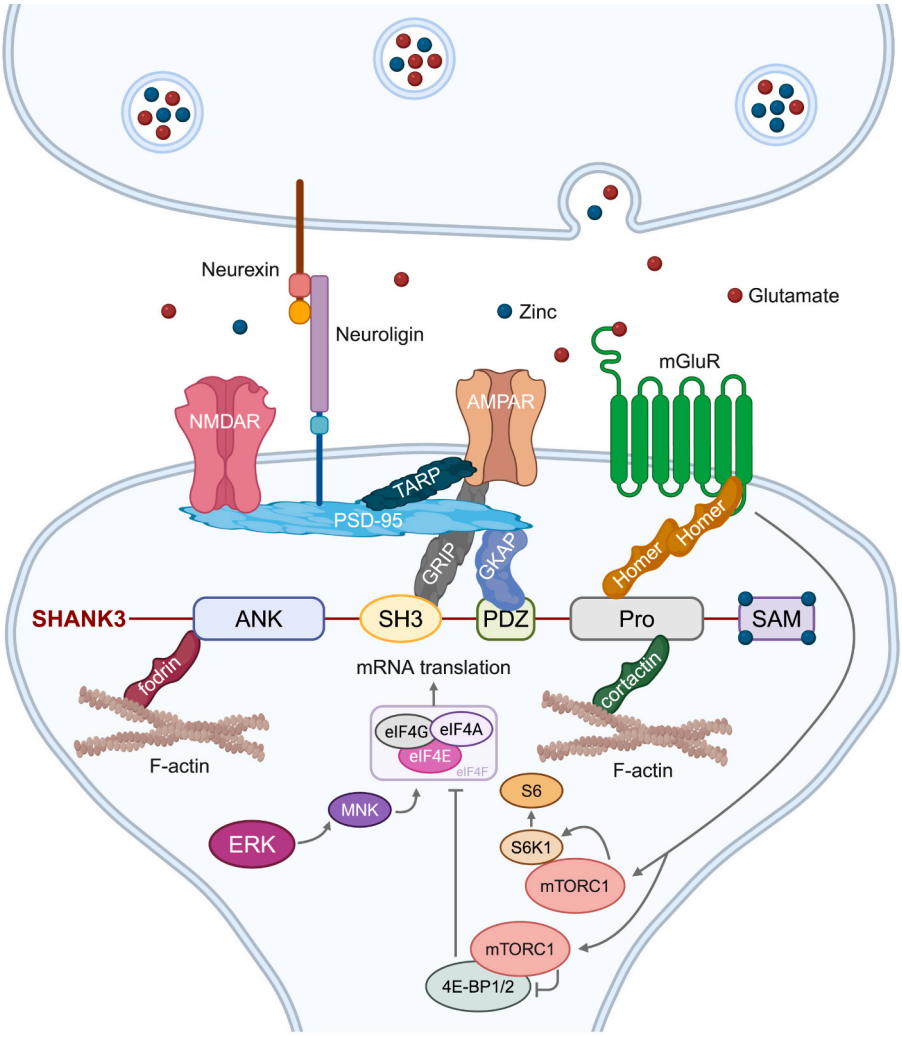

Fig. 1. Schematic representation of the hypothetical connection between SHANK3 and mRNA translation. SHANK3 plays a critical role in synaptic development and brain function and contains five conserved domains to interact with synaptic-associated proteins. The domains from the N-terminus to the C-terminus are an ANK domain, which interacts with actin filaments through α-fodrin. A SH3 domain mediates binding to the AMPAR through GRIP. A PDZ domain binds to GKAP, which interacts with PSD-95 and, consequently, with NMDAR, neuroligin, and AMPAR. A Pro domain links mGluR with actin filaments through Homer and cortactin proteins. A SAM domain is involved in the polymerisation of Shank molecules in a zinc-dependent manner. SHANK3 impacts receptors upstream of the mTORC1 and MAPK/ERK signalling pathways, such as mGluRs and NMDARs.

matter abnormalities in both PMS patients and mouse models (Fischer et al., 2024; Jesse et al., 2020; Malara et al., 2022). These findings show that SHANK3 contributes to neural circuit functioning not only through synaptic mechanisms but also by supporting axon-glial communication and myelin integrity.

SHANK3 exists, according to Ensembl, in 12 transcript variants in humans and 10 in mice, due to alternative promoter usage and splicing (Ensembl, 2025). SHANK3 exhibits disparate expression patterns across brain regions and cell types in mice and is regulated differentially in developmental stages and neuronal activity (Wang et al., 2014). The isoforms differ in their subcellular localisation and impact on density and length of dendritic spines. Mutations and deletions in *SHANK3* engender synaptic signalling and plasticity abnormalities, which underlie behavioural deficits in PMS (Cammarata-Scalisi et al., 2022). *SHANK3* aberrations are found in 1–2 % of patients with ASD and up to 2 % of patients with ID, rendering it as one of the common monogenic causes of ASD and ID (Cammarata-Scalisi et al., 2022; Leblond et al., 2014).

Five established *Shank3* knockout (KO) mouse models recapitulate the clinical features observed in PMS and ASD: social interaction impairments, repetitive behaviour, anxiety, epilepsy, and memory impairments (Delling and Boeckers, 2021; Peça et al., 2011). Short-term and long-term memory have been studied in these models, yielding contradicting results for several reasons: different genetic backgrounds, age of the mice, and variable behavioural protocols (Cope et al., 2023; Dhamne et al., 2017; Jaramillo et al., 2016). In this study, we used the *Shank3B*$^{-/-}$ mouse model (Peça et al., 2011), in which exons 13 to 16 of the *Shank3* gene are deleted, resulting in the loss of the PDZ domain and the disruption of Shank3 isoforms that contain this domain. These mice exhibit increased self-grooming, deficits in social interaction, hypomobility, decreased frequency of ultrasonic vocalisations (USVs), and alterations in medium spiny neurons (MSNs) and postsynaptic density composition in the striatum (Dhamne et al., 2017; Pagani et al., 2019; Peça et al., 2011).

The insulin-growth factor 1 (IGF-1) and insulin were investigated as possible treatments for PMS (Kolevzon et al., 2022; Zwanenburg et al., 2016). IGF-1 administration corrected AMPA signalling, long-term potentiation, and motor performance in a PMS mouse model, and restored excitatory synaptic transmission in induced pluripotent stem cell-derived neurons from patients with PMS (Bozdagi et al., 2013; Shcheglovitov et al., 2013). Consequently, subcutaneous injection of IGF-1 improved repetitive behaviour and hyperactivity in children from 5 to 15 years old, while intranasal insulin engendered improvements in social skills and cognition only in children older than three years (Kolevzon et al., 2022; Zwanenburg et al., 2016). The high cost, limited accessibility, and need for injection of IGF-1, along with the insulin-related side effect of hypoglycemia, limit their utility, highlighting the need for more accessible alternatives (Amiel, 2021; Cammarata-Scalisi et al., 2022; Kolevzon et al., 2022).

The reported efficacy of targeting insulin signalling to treat PMS prompted us to examine metformin, an FDA-approved drug for type 2 diabetes, as a therapeutic drug. Metformin suppresses the mTORC1 and MAPK/ERK pathways, which are often hyperactivated in disorders with a high incidence of ASD (Gantois et al., 2019). Gantois et al. reported that chronic administration of metformin decreased phosphorylation of MAPK/ERK and eukaryotic initiation factor 4E (eIF4E), and corrected core phenotypes in the fragile X syndrome (FXS) mouse model, such as repetitive behaviour and social interaction (Gantois et al., 2017). The timing of metformin administration plays a critical role in modulating signalling pathways. Specifically, metformin treatment started at birth in the FXS mouse model, but not in adulthood, rescued mTORC1 signalling (Choi et al., 2024; Gantois et al., 2017). As for the FXS mouse model, studies in *Shank3* KO mouse models reported increased cerebral protein synthesis and mTORC1 activity (Mencer et al., 2021; Torossian et al., 2021). Given the promising results, metformin is currently in clinical trials for treatment of FXS (Biag et al., 2019; Dy et al., 2018; U.S. National Library of Medicine, 2025).

This study reports autistic-like behaviours, memory impairments, and increased mTORC1 signalling in *Shank3B*$^{-/-}$ mice. Administration of metformin from birth corrected behavioural impairments, and normalised the mTORC1 pathway and striatal synaptosomal proteins. Together, these findings should advance effective and accessible treatments for PMS.

2. Methods

2.1. Mice and treatment

Male WT and *Shank3B*$^{-/-}$ mice on a C57BL/6J background (Jackson Laboratories, Shank3^{tm2Gfng}, catalogue #017688) were used (Peça et al., 2011). Homozygous WT and *Shank3B*$^{-/-}$ mice were bred separately, and offspring were generated from breeding pairs of the same genotype. Therefore, WT and *Shank3B*$^{-/-}$ mice used in this study were non-littermates. Mice were housed in groups of up to five per cage (Plexiglas cage of 19.1 cm × 29.2 cm × 12.7 cm, Allentown) with Teklad corncob bedding (Envigo) and one square of nesting material (Nestlets, Ancare), without additional environmental enrichment. Animals had ad libitum access to food (Teklad irradiated global soy protein-free extruded rodent diet, Inōtiv) and water and were maintained under standard temperature (20–21 °C) and humidity (55 %) conditions and 12 h:12 h light-dark cycles (7:00–19:00 h, light period) in a specific pathogen-free (SPF) facility.

Metformin (5 mg/mL, Sigma-Aldrich, 317240) or vehicle (water) was administered daily starting no later than 1 day after birth. Before weaning, mice received metformin through the maternal milk of their respective mother, who received metformin through the drinking water (Hale et al., 2002). Although this results in lower exposure during the lactation period, consistent with the milk-to-plasma ratio of 0.35 in humans, this approach ensures treatment starts early in development. After weaning, mice were treated with metformin or vehicle directly through their drinking water. This dosing was chosen based on Memmott et al., who reported that mice receiving 5 mg/mL achieved a plasma concentration of 1.70 μg/mL, which corresponds to steady-state concentrations in humans (0.5–2 μg/mL) (Memmott et al., 2010). Mice were allocated to vehicle or metformin groups at birth, with assignments balanced to obtain similar group sizes.

Mice were monitored at least once per week by trained personnel to assess general health and well-being before, during, and after the experiments. Procedures followed the Canadian Council on Animal Care guidelines and were approved by McGill University.

2.2. Behavioural tests

Prior to starting behavioural tests, mice were transferred to a conventional animal facility and allowed to acclimate for at least 1 week to minimise environmental stress. To further reduce handling-related stress, mice were handled for three consecutive days for 1 min each day. Tests were carried out in the morning during the light cycle, except when otherwise indicated. Mice were acclimated to the behavioural testing room for at least 30 min before each test, and for a minimum of 1 h for the three-chamber assay. During behavioural testing, the order of mice was intercalated across genotype and treatment groups to minimise order effects. Between each mouse, each object or testing apparatus was cleaned with Versa-Clean (Fisher Scientific). Testing and scoring were performed in a blinded manner. The same cohorts of mice were used for the open field, NOL, and NOR tests, which were performed sequentially and then combined for analysis. All other behavioural assays were conducted in separate groups of mice, with one cohort per test, except for the three-chamber test, which was assessed in two independent cohorts.

2.2.1. Self-grooming test

A Plexiglas cage (19.1 cm × 29.2 cm × 12.7 cm) with no valve, similar to the home cage, was filled with approximately 1 cm of fresh bedding material (Teklad Corncob Bedding, Envigo) but no nesting material, as previously described (Huang et al., 2024). All trials were recorded using a camera in front of the cage. Mice (males aged 8–10 weeks) were placed in the Plexiglas cage for 20 min. The first 10 min were considered the habituation phase, while the remaining time was used for the self-grooming data. Grooming behaviour was analysed as the time spent grooming and the number of grooming bouts. A grooming bout is considered as any instance of grooming activity, regardless of whether the mouse completes some or all four stages of grooming (from initial paw licking around the nose and whiskers to body and tail grooming) (Kalueff et al., 2015). Scoring was carried out manually using a stopwatch. Data were analysed with a two-way ANOVA followed by Bonferroni's multiple comparisons test.

2.2.2. Three-chamber sociability and preference for social novelty test

A three-chambered Plexiglass apparatus consisting of a central chamber (36 cm × 28 cm × 30 cm) separated from two side chambers (each measuring 29 cm × 28 cm × 30 cm) by Plexiglas walls (Stoelting Co.) was used as previously described (Rein et al., 2020). The chambers were interconnected through doorways, each fitted with a removable sliding door. Additionally, a wire cage was placed in each side chamber to house a stimulus. All trials were recorded using an overhead camera for later analysis. In each phase of the experiment, the test mouse (male aged 9–11 weeks) was placed in the central chamber and, upon opening the doors, the mouse was allowed to explore freely for 10 min. The test mouse was returned to its home cage for a 5-min break between each phase. During the habituation phase, the wire cages in the side chambers were left empty. In the pre-test phase, a single paper ball was placed in each wire cage to acclimate the mouse to the presence of an object within them. Subsequently, in the social preference phase, one wire cage hosted a social stimulus (Stranger 1), while the opposite wire cage contained a non-social stimulus (a purple wooden cube). In the final phase (social novelty), the non-social stimulus was replaced with a novel mouse (Stranger 2); thus, the initial social stimulus, Stranger 1, became the familiar mouse. Stranger mice used as stimuli were age-, sex-, and body weight-matched C57BL/6 J mice. The wire cages containing Stranger 1 or the object were alternated across test mice to ensure variability. Time spent sniffing the wire cages was scored manually employing a stopwatch. Exploration was scored when the mouse oriented its nose toward the wired cup with active investigation (sniffing, touching, or close inspection), as visually assessed by the experimenter. The social preference index was determined by the amount of time spent exploring the social stimulus compared to the total time spent exploring both stimuli. The social novelty index was assessed based on the time spent exploring the Stranger 2 mouse relative to the total time exploring both stranger mice. An exclusion criterion of a minimum exploration time of 20 s was applied as previously described (Leger et al., 2013). Data were analysed with a two-way ANOVA followed by Bonferroni's multiple comparisons test.

2.2.3. Ultrasonic vocalisation test

WT females of the same age and C57BL/6 J background as the male test mouse (aged 7–11 weeks) were used as stimuli. On the morning of the ultrasonic vocalisation (USV) test, vaginal smears from each female stimulus were taken to determine their status in the oestrous cycle by holding their tail and collecting a vaginal sample with a Q-tip, previously soaked in PBS. The samples were stained with crystal violet (1 min in crystal violet and 1 min in double-distilled water, three times each), let to dry, and analysed under the microscope. Only the females in full oestrus (predominantly cornified squamous epithelial cells found in densely packed clusters) were selected as stimuli (McLean et al., 2012). After that, a clean cage with approximately 1.5 cm of bedding material with a grid but without a lid was set up in an isolated chamber with an ultrasound microphone (Avisoft-UltraSoundGate condenser ultrasound microphone CM16/CMPA; Avisoft Bioacoustics) suspended 20 cm above the cage. The male test mouse was put in the cage, and after 10 min of habituation, a female in full oestrus was introduced into the cage. The two mice were then allowed to interact for 5 min while being recorded using Avisoft-RECORDER software (version 4.2.27; Avisoft Bioacoustics; RRID:SCR_014436). One new cage was used for each test mouse, and each female stimulus interacted with no more than three male mice a day, with at least half an hour of resting between tests, as previously described (Ferhat et al., 2016). The data were analysed with the Avisoft-SASLab Pro software (version 5.2.12; Avisoft Bioacoustics) and sorted into calls per minute and USV duration using a self-made Python file (Marsal-García, 2024). Data were analysed with a two-way ANOVA followed by Bonferroni's multiple comparisons test.

2.2.4. Novel object location

Mice (males aged 17–21 weeks) were individually placed, for 4 days, in a white-wall box (50 cm × 50 cm × 30 cm) with a star on one wall as a position clue. Each day, except for Day 4, included one testing session in the morning and one in the afternoon, and, in between sessions, mice were returned to their home cage for rest and hydration. On Day 1 (habituation), mice were placed in the empty testing apparatus for 10 min in the morning and afternoon to acclimate to the environment. On Days 2 and 3 (training), two identical objects were positioned in the centre of the box, and the mice were returned to the apparatus for 10 min during each session, in the morning and in the afternoon, to explore the objects. On Day 4 (testing), 24 h after the last training session, one of the objects used on Days 2 and 3 was moved to a novel place, and the mice were reintroduced to explore this setting for 10 min. The novel location was counterbalanced across test mice by varying which object was moved and its specific position within the box. This ensured that the location of the novel object differed between trials, minimising positional bias. All trials were recorded using a camera on top of the box for later analysis with EthoVision XT (RRID:SCR_000441). Object exploration was quantified as the time spent interacting with the object. We defined an exploration zone as a 10-cm diameter circular region centred on each object, following standard EthoVision procedures. This zone included the object itself. Exploration time was analysed when the mouse's nose point was detected within this defined zone. Preference for the novel location, also referred to as the discrimination index, was calculated as the difference in the time spent exploring the novel object location and the time spent exploring the familiar object location relative to the total time spent exploring both locations (Huang et al., 2025). An exclusion criterion of a minimum exploration time of 20 s was applied as previously described (Leger et al., 2013). Data were analysed with a mixed-design three-way ANOVA or a non-parametric ANCOVA using the Quade test, followed by Bonferroni's multiple comparisons test.

2.2.5. Novel object recognition

Mice (males aged 18–22 weeks) were individually placed, for 4 days, in a white-wall box (50 cm × 50 cm × 30 cm) with a star on one wall as a position clue. In the novel object recognition (NOR) test, each day included only one testing session in the morning, contrary to the novel object location (NOL) test. On Day 1 (habituation), the mouse was placed into the empty box for 10 min to explore the apparatus. On Days 2 and 3 (training), two identical objects (familiar) were placed in the middle of the box, and the mouse was put back in the arena for 10 min to explore the objects. On Day 4 (testing), one of the objects was changed with a different one. The mouse was then reintroduced to explore the novel object. As similarly described for the novel location test, the location of the novel object here varied across test mice to ensure minimal positional bias. All trials were recorded using a camera on top of the box for later analysis with EthoVision XT (RRID:SCR_000441). Object exploration was quantified as the time spent interacting with the object. We defined an exploration zone as a 10-cm diameter circular

region centred on each object, following standard EthoVision procedures. This zone included the object itself. Exploration time was analysed when the mouse's nose point was detected within this defined zone. Preference for the novel object, or discrimination index, was calculated as the difference in the time spent exploring the novel object and the time spent exploring the familiar object relative to the total time spent exploring both objects (Huang et al., 2025). An exclusion criterion of a minimum exploration time of 20 s was applied as previously described (Leger et al., 2013). Data were analysed with a mixed-design three-way ANOVA or a non-parametric ANCOVA using the Quade test, followed by Bonferroni's multiple comparisons test.

2.2.6. Open field locomotion

Mice (males aged 18–22 weeks) were individually placed in a white-wall box (50 cm × 50 cm × 30 cm) with a star on one wall as a position clue for 10 min (Wiebe et al., 2020). All trials were recorded using a camera on top of the box for later analysis with EthoVision XT (RRID: SCR_000441). The time spent moving (mobility) and the time in the centre zone versus the outer zone (anxiety) were measured. Data were analysed with the non-parametric two-sided Mann-Whitney *U* test (not normally distributed: $p < 0.05$ for the Shapiro-Wilk test) for anxiety and a two-way ANOVA for mobility.

2.2.7. Light-dark box test

The test apparatus consisted of a dark black enclosed chamber and a light, open-top white chamber (40 cm × 40 cm × 20 cm) connected through a small opening. A bright light (~390 lx) was placed above the open chamber (Gantois et al., 2017). Mice (males aged 9–10 weeks) were put into the light side and were free to explore the apparatus for 10 min while being recorded from the top. The time spent in each chamber was scored manually employing a stopwatch. Data were analysed with the non-parametric two-sided Mann-Whitney *U* test (not normally distributed: $p < 0.05$ for the Shapiro-Wilk test).

2.2.8. Elevated plus maze

The test apparatus consisted of two closed arms and two open arms oriented as a plus sign and elevated from the ground (Stoelting). Sawdust was scattered on the surface to provide contrast between the mouse and the maze and give the mouse some traction. The sawdust was replaced as needed between mice. Mice (males aged 10–15 weeks) were placed in the centre of the plus maze and were free to explore all the arms for 5 min while being recorded from the top (Wiebe et al., 2020). The time spent in open and closed arms was used as a measure of generalised anxiety. Scoring was carried out manually using a stopwatch. Data were analysed with the non-parametric two-sided Mann-Whitney *U* test (not normally distributed: $p < 0.05$ for the Shapiro-Wilk test).

2.3. Electrophysiology

Hippocampal slices were obtained from P25-P40 old WT or *Shank3B*$^{-/-}$ mice. Mice were deeply anaesthetised with isoflurane and killed by decapitation. Slices (400 μm) were cut on a vibratome (Leica Microsystems, VT1200S) in a sucrose-based solution containing the following (in mm): 280 sucrose, 26 $NaHCO_3$, 10 glucose, 1.3 KCl, 1 $CaCl_2$, and 10 $MgCl_2$ and were transferred at 32 °C in regular artificial cerebrospinal fluid (ACSF) containing the following (in mm): 124 NaCl, 5 KCl, 1.25 NaH_2PO_4, 2 $MgSO_4$, 26 $NaHCO_3$, 2 $CaCl_2$, and 10 glucose saturated with 95 % O_2/5 % CO_2 (pH 7.3, 300 mOsm) for 15 min before resting at room temperature (RT) for 1 h in oxygenated (95 % O_2/5 % CO_2) ACSF. For recording, slices were transferred to a temperature-controlled (32 °C) chamber with oxygenated ACSF. To assess group I metabotropic glutamate receptor (mGluR)-dependent long-term depression (LTD), slices were placed into a heated (32 °C) recording chamber of an upright microscope (DM LFSA Microsystems) and perfused continuously with regular ACSF. 3,5-dihydroxyphenylglycine (DHPG) (100 μM) was applied for 5 min after baseline recording. Field excitatory postsynaptic potentials (fEPSPs) were recorded in the stratum radiatum, a layer of the hippocampal CA1 region, using glass microelectrodes filled with 3 M NaCl. GABAA receptor-mediated inhibition was blocked with 100 μm picrotoxin, and the area CA1 was surgically isolated from CA3 to avoid epileptiform activity. fEPSPs were elicited at 0.1 Hz by a digital stimulator fed by a stimulation isolator unit. All data analyses were performed with custom-written software in Igor Pro 8 (Wavemetrics). The fEPSP slope was measured as an index of synaptic strength. Data were analysed with a standard two-sided *t*-test.

2.4. Synaptosome preparation

Striata from mice (males aged 8–11 weeks) were isolated, frozen in liquid nitrogen, and kept at −80 °C. Synaptosome extraction was performed using the Syn-PER™ Synaptic Protein Extraction Reagent (87,793, Thermo Fisher Scientific) following the manufacturer's instructions. Ice-cold Syn-PER Reagent with protease and phosphatase inhibitors (469315901, Roche; P5726-5ML, P0044-5ML, Sigma-Aldrich) was used to homogenise the striatum tissue. The homogenate was centrifuged at 1200 x *g* for 10 min at 4 °C. The pellet with the debris was discarded, and the supernatant was further centrifuged at 15000 x *g* for 20 min at 4 °C. The cytosolic fraction (supernatant) and the synaptosome pellet were washed separately by centrifuging at 15000 x *g* for 10 min at 4 °C. The synaptosome pellet was suspended in ice-cold radioimmunoprecipitation assay (RIPA) buffer (R0278, Sigma-Aldrich) containing protease and phosphatase inhibitors (as above) and was used for subsequent Western blotting analysis.

2.5. Western blotting

Hippocampus, prefrontal cortex, and striatum were isolated from each mouse (males aged 8–11 weeks), frozen in liquid nitrogen, and kept at −80 °C. Ice-cold RIPA buffer (R0278, Sigma-Aldrich) containing protease inhibitors mixture and phosphatase inhibitors (469315901, Roche; P5726-5ML, P0044-5ML, Sigma-Aldrich) was used to homogenise the samples for protein extraction.

Protein extracts were obtained from whole-tissue homogenates (RIPA buffer) or synaptosome fractions (see Synaptosome preparation) and were processed for Western blotting as described below. Extracts were denatured by heat (5 min, 95 °C), separated by 7 % or 10 % SDS-PAGE, transferred onto nitrocellulose membranes, and immunoblotted. Membranes were stripped in 25 mM-glycine-HCl, pH 2.0 and 1 % SDS for 30 min at room temperature, followed by three TBS-T washes (TBS, 0.1 % Tween 20) before reprobing. Immunoreactivity was detected by enhanced chemiluminescence (plus-ECL, PerkinElmer, Inc.) after exposure to X-ray film (Denville Scientific, Inc.). Quantification of immunoblots was performed with ImageJ (National Institutes of Health). Glyceraldehyde 3-phosphate dehydrogenase (GAPDH), β-tubulin or β-actin were used as a loading control for total proteins. Phosphoproteins were normalised against their non-phosphorylated forms. Antibodies are described in Supplementary Table 2. Full western blots are available in Supplementary material 2.

2.6. mRNA extraction and RT-qPCR

Mice (males aged 8–11 weeks) hippocampus, prefrontal cortex, and striatum were isolated, frozen in liquid nitrogen, and kept at −80 °C. Total mRNA was extracted using Trizol (Invitrogen) following the manufacturer's instructions. Equal amounts of mRNA (1 μg) were reverse transcribed following the SuperScript III Reverse Transcriptase protocol (18080044, Invitrogen) using oligo$(dT)_{18}$. mRNA abundance was determined through the CFX Connect real-time PCR (qPCR) system (Bio-Rad) and CFX Maestro Software 1.1 (Bio-Rad) using 2× Universal SYBR Green Fast qPCR Mix (ABclonal). All samples were done in duplicate, and *β-actin* was used for normalisation. A comparative Ct

method was used for quantification. Primer sequences are reported in Supplementary Table 3.

2.7. Statistical analysis

Data analysis was performed using SPSS Version 29, and the results are presented as mean ± standard error of the mean (SEM). A detailed summary of the statistical results and the tests employed (*t*-test, Welch's *t*-test, Mann-Whitney *U* test, two-way ANOVA, mixed-design two-way ANOVA, mixed-design three-way ANOVA, and ANCOVA using the Quade test) can be found in Supplementary Table 1. Statistical significance was considered if $p < 0.05$. Group sizes were chosen based on prior experience in our laboratory and on established sample sizes in the literature for similar behavioural and molecular assays, ensuring feasibility and sufficient power to detect meaningful effects.

To account for potential differences in overall activity levels due to hypomobility in the mice during the NOL and NOR tests, we performed a non-parametric Analysis of Covariance (ANCOVA) using the Quade test (Mina et al., 2018). The dependent variable was the discrimination index of the two objects explored by the mice, and the between-subject factors were Genotype and Treatment. Total exploration time, which measures the time spent exploring both objects, was used as a covariate to control for variations in general activity levels among the mice. Ranking procedures were applied to the dependent variable and covariate to meet the assumptions of the Quade test. Residuals from the ranked dependent variable were analysed to assess the effects of genotype and treatment while adjusting for total exploration time.

Given the ultrasonic vocalisation test's small sample size ($n = 7$–8) and the relatively narrow range of observed values (0 to 0.03), we employed the ROUT test with a Q value of 10 % for outlier detection, which excluded one mouse.

GraphPad Prism 10.4.1 (GraphPad Software) and Microsoft Excel (Microsoft 365, Microsoft Corporation) were used to generate the graphs.

3. Results

First, we confirmed that male *Shank3B*$^{-/-}$ mice did not express *Shank3* mRNA and protein in the hippocampus, prefrontal cortex, and striatum (Supplementary Fig. 1A-F; mRNA levels: hippocampus: $p < 0.001$; prefrontal cortex: $p < 0.001$; striatum: $p < 0.001$, and protein levels: hippocampus: genotype main effect: $p < 0.001$; prefrontal cortex: genotype main effect: $p < 0.001$; striatum: genotype main effect: $p < 0.001$).

As metformin treatment engenders weight loss in diabetic patients, people with high waist-to-hip ratios, obese, and young individuals with ASD (Anagnostou et al., 2016; Dy et al., 2018; Fontbonne et al., 1996; Glueck et al., 2001; Yerevanian and Soukas, 2019), we monitored mouse body weight. Adult (10–13 weeks old) wild-type (WT) and *Shank3B*$^{-/-}$ mice treated with metformin (treatment regimen: Supplementary Fig. 2A) showed a similar decrease in weight compared to the vehicle-treated groups, 11.3 % and 10.5 %, respectively (Supplementary Fig. 2B; treatment main effect: $p < 0.001$). Since body weight reduction was also observed in the WT group, no adjustment was made to our experimental design.

3.1. *Shank3B*$^{-/-}$ mice displayed autistic-like behaviours that were corrected by metformin treatment

Given the high incidence (80 %) of ASD in PMS patients, we examined male mice for core ASD phenotypes: repetitive behaviour and social interactions (Cammarata-Scalisi et al., 2022) (Fig. 2A). Self-grooming, which is associated with striatal functioning, was measured to assess repetitive behaviour (Kazdoba et al., 2016; Piantadosi et al., 2024). *Shank3B*$^{-/-}$ mice showed a 2.52 ± 0.70-fold increase in duration ($p < 0.001$) and a 2.18 ± 0.61-fold increase in frequency ($p < 0.001$) of self-grooming (Fig. 2B, C). Time spent grooming ($p < 0.001$) and the number of grooming bouts ($p < 0.001$) in *Shank3B*$^{-/-}$ mice were reduced to WT levels by metformin administration (Fig. 2B, C).

Individuals with PMS manifest impaired social skills, which can be modelled and analysed in rodents using the three-chamber test (Cammarata-Scalisi et al., 2022; Crawley, 2004; Kazdoba et al., 2016). *Shank3B*$^{-/-}$ mice exhibited a ~25.5 % reduction in social preference index compared to WT mice (Fig. 2D; $p = 0.006$), indicating decreased social interaction. No difference was found in the social novelty index (Fig. 2E; $p = 0.696$), indicating normal social memory or novelty preference. Metformin treatment from birth corrected the social preference impairment observed in *Shank3B*$^{-/-}$ mice (Fig. 2D; $p = 0.037$).

To examine delayed development and speech, which are core features of PMS and ASD, we analysed USVs during social interaction, mirroring aspects of human communication (Cammarata-Scalisi et al., 2022; Crawley, 2004; Morrel et al., 2023; Yao et al., 2023). *Shank3B*$^{-/-}$ mice exhibited a 1.80 ± 0.45-fold reduction in USV duration (Fig. 2F; $p = 0.016$) and a 5.23 ± 5.05-fold decrease in the number of calls per minute (Fig. 2G; genotype main effect: $p = 0.034$). Metformin treatment increased USV duration 2.10 ± 0.47-fold ($p = 0.003$) and partially corrected (4.12 ± 4.22-fold) call frequency (treatment main effect: $p = 0.156$) in *Shank3B*$^{-/-}$ mice (Fig. 2F, G).

Taken together, metformin corrected three core autistic-like behavioural deficits in *Shank3B*$^{-/-}$ mice.

3.2. Metformin corrected learning and memory deficits in *Shank3B*$^{-/-}$ mice

Since SHANK3 plays a critical role in the development, function, and plasticity of synapses, memory was assessed in male *Shank3B*$^{-/-}$ mice using novel object location (NOL) and novel object recognition (NOR) tests (Monteiro and Feng, 2017; Sala et al., 2015; Vogel-Ciernia and Wood, 2014) (Fig. 3A).

WT and *Shank3B*$^{-/-}$ mice were subjected to the NOL test. As expected, WT mice showed a 1.35 ± 0.19-fold increase in exploration time with the object in the novel location ($p = 0.006$), while *Shank3B*$^{-/-}$ mice did not show a preference as they spent equal time exploring both the object in the familiar location and the object in the novel location (Fig. 3B; $p = 0.222$). After adjusting for total exploration time, we found a statistically significant impairment in hippocampal-dependent memory among *Shank3B*$^{-/-}$ mice, with a 151.14 % decrease compared to WT mice (Fig. 3C; $p = 0.017$).

Because metformin enhances memory (Gantois et al., 2019; Ishola et al., 2020; Monyak et al., 2017; Pourfridoni et al., 2024), we examined whether it could ameliorate the memory deficit in *Shank3B*$^{-/-}$ mice. Indeed, the impaired memory observed in *Shank3B*$^{-/-}$ mice was effectively rescued as they spent 2.28 ± 0.49-fold more time exploring the object in the novel compared to the familiar location (Fig. 3B; $p < 0.001$), and a significant 4.77 ± 4.39-fold increase in object-location preference (Fig. 3C; $p < 0.001$).

In the NOR test, *Shank3B*$^{-/-}$ mice, like WT mice, explored the novel object 1.53 ± 0.41-fold more than the familiar one (Fig. 3D; object main effect: $p < 0.001$). After accounting for the overall time spent exploring, *Shank3B*$^{-/-}$ mice presented a similar discrimination index as WT mice, indicating no recognition memory impairment (Fig. 3E; genotype main effect: $p = 0.608$).

Several studies reported hypoactivity in *Shank3B*$^{-/-}$ mice (Angelakos et al., 2019; Balasco et al., 2022; Dhamne et al., 2017; Liu et al., 2021; Peixoto et al., 2019). To examine this phenotype in our model, we measured the total distance travelled in the open field. *Shank3B*$^{-/-}$ mice travelled a 1.63 ± 0.15-fold shorter distance than the WT group (Fig. 3F; genotype main effect: $p < 0.001$), in agreement with previous reports. Metformin failed to correct the hypoactivity of *Shank3B*$^{-/-}$ mice (Fig. 3F; treatment main effect: $p = 0.650$). Due to their hypomobility, the discrimination index described in NOL and NOR was analysed using a non-parametric ANCOVA (Quade test), with total

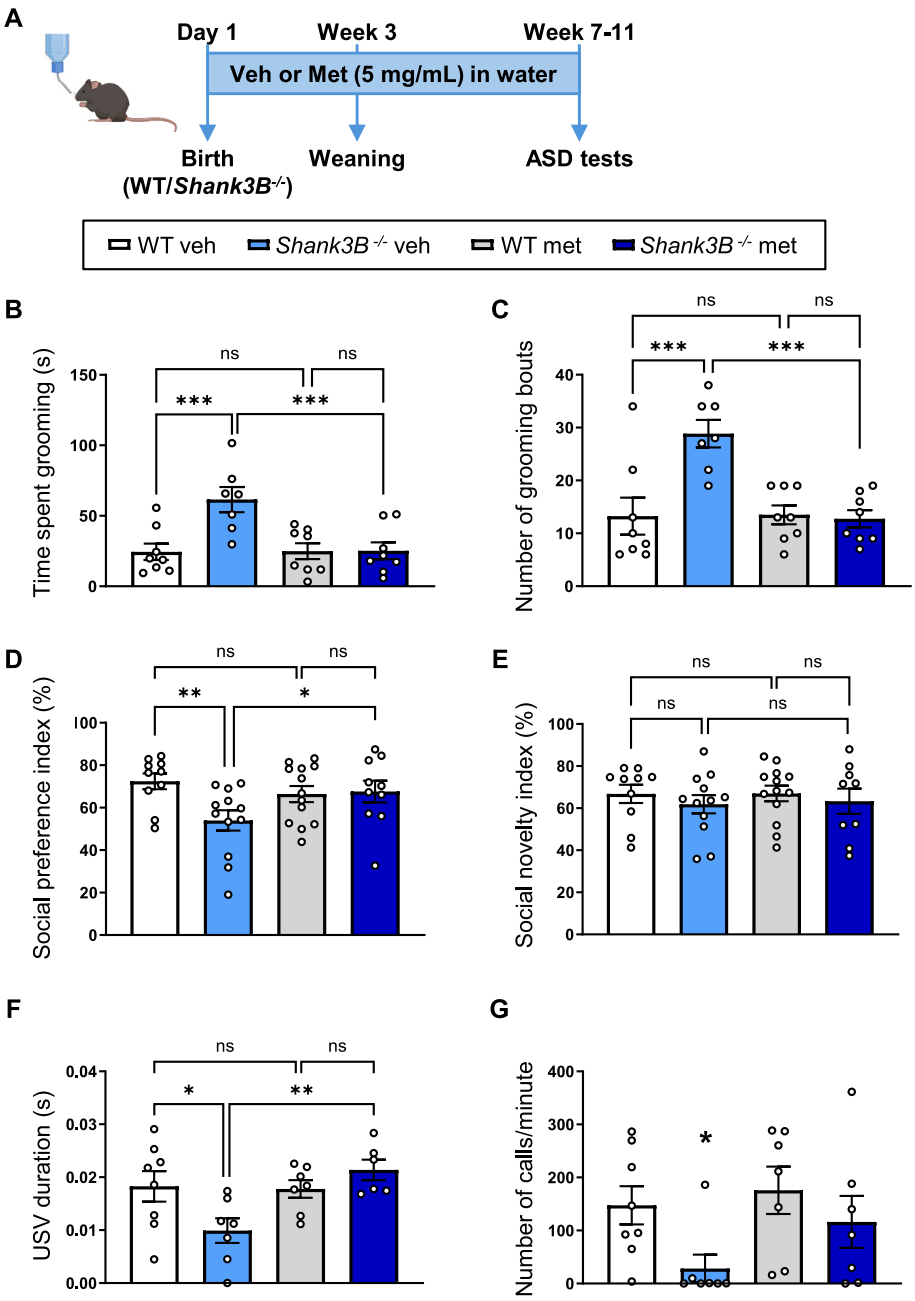

Fig. 2. Metformin corrected autistic-like behaviours in *Shank3B*$^{-/-}$ mice. (A) Mice treated from birth with vehicle (veh) or metformin (met) underwent autistic-like behavioural testing at 7–11 weeks old. Repetitive behaviour ($n = 7$–8) was assessed by measuring (B) the time spent grooming and (C) the number of grooming bouts. (D) Social preference ($n = 10$–13) was evaluated by the three-chamber test, expressed as the ratio of time spent with the social stimulus (stranger 1) compared to the total time spent with both the social and non-social stimuli. (E) Social novelty ($n = 9$–13) was assessed in the three-chamber test by calculating the ratio of time spent with the novel mouse (stranger 2) compared to the total time spent with both stranger 2 and the familiar mouse (stranger 1). USVs ($n = 6$–8) were measured as (F) USV duration and (G) number of calls per minute. In (G), the genotype main effect was significant, but the genotype × treatment interaction was not; the asterisk above the KO vehicle bar indicates a significant genotype effect, showing a reduction in calls compared to WT. Each point represents data from an individual mouse, and all values (B-G) are shown as mean ± SEM, ***$p < 0.001$, **$p < 0.01$, *$p < 0.05$, ns = not significant versus all other groups; calculated by two-way ANOVA with Bonferroni's post hoc test (statistical analysis is shown in Supplementary Table 1).

exploration time included as a covariate to control for hypomobility-related differences in overall activity levels (Fig. 3C, E). We, therefore, conclude that the observed differences in the discrimination index of the NOL and NOR tests are directly associated with the genetic and treatment variables studied and not merely a result of overall activity levels.

To study synaptic plasticity in *Shank3B*$^{-/-}$ mice, we measured group I mGluR-dependent long-term depression (mGluR-LTD) in the hippocampus (Supplementary Fig. 3A). No difference in hippocampal mGluR-LTD between *Shank3B*$^{-/-}$ and WT mice was found (Supplementary Fig. 3B, C; $p = 0.446$).

The results underscore the critical role of *Shank3* in memory processes. *Shank3* deletion results in hippocampal-dependent memory impairment in mice, which is corrected by metformin administration from birth.

3.3. *Shank3B*$^{-/-}$ mice did not exhibit anxiety behaviour

To exclude anxiety as a confounding factor in the interpretation of

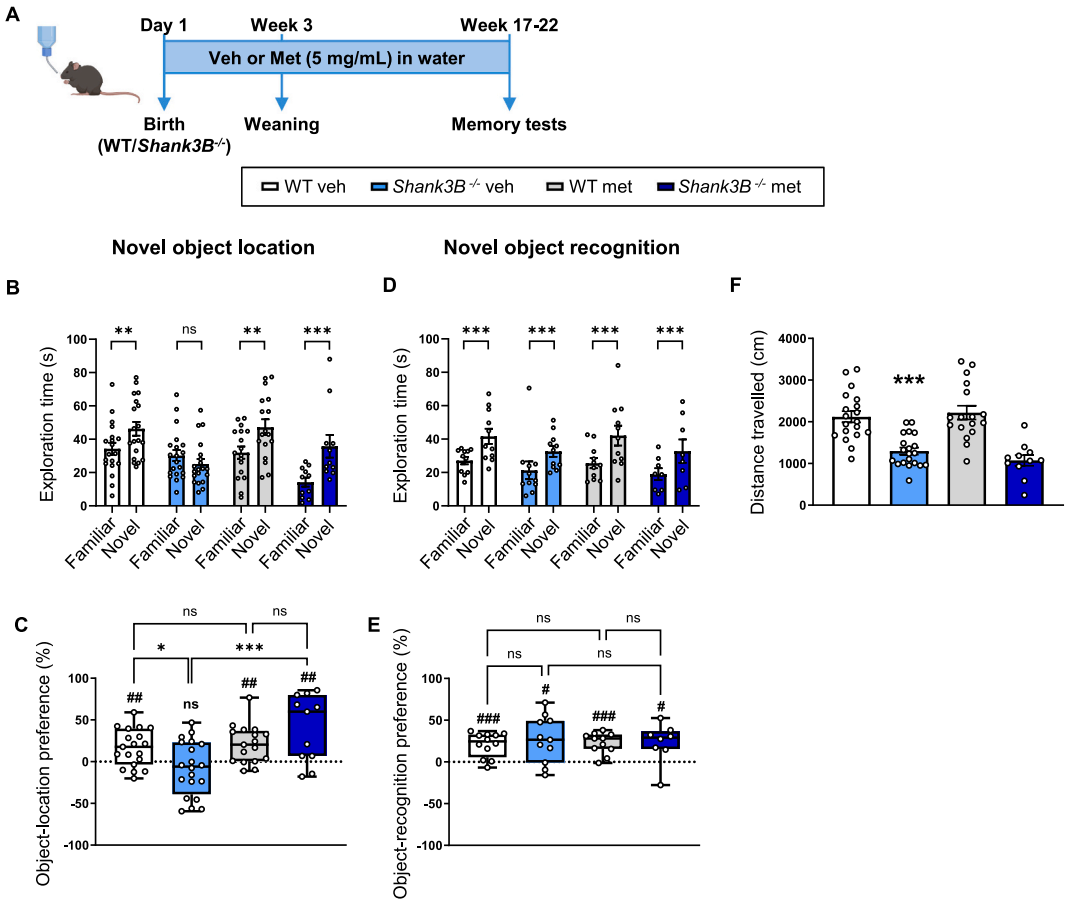

Fig. 3. Memory impairment in *Shank3B*$^{-/-}$ mice was rescued by metformin treatment. (A) Mice treated from birth with vehicle (veh) or metformin (met) underwent memory tests at 17–22 weeks old. Memory was assessed using two parameters: the difference in exploration time (B) between the familiar and novel location in the NOL test (n = 11–20) and (D) between the familiar and novel object in the NOR test (n = 8–12), as well as the adjusted discrimination index for the (C) NOL and (E) NOR tests in WT and *Shank3B*$^{-/-}$ mice. The adjusted discrimination index accounted for total exploration time as a covariate to control hypomobility-related differences in overall activity levels. (F) Mobility (n = 11–20) was measured as the distance travelled in the open field test. In (C, E), the original discrimination index values were used for plotting to preserve negative values observed in the raw data. In (F), the genotype main effect was significant, but the genotype × treatment interaction was not; the asterisk above the KO vehicle bar indicates a significant genotype effect, showing a reduction in distance travelled compared to WT. Each point represents data from an individual mouse, and all values (B—F) are shown as mean ± SEM, ***$p < 0.001$, **$p < 0.01$, *$p < 0.05$, $^{\#\#\#}p < 0.001$, $^{\#\#}p < 0.01$, $^{\#}p < 0.05$, ns = not significant versus all other groups (*) or versus 0 ($^{\#}$); calculated by (B, D) mixed-design three-way ANOVA with Bonferroni's post hoc test, (C, E) Quade test with Bonferroni's post hoc test, or (F) two-way ANOVA (statistical analysis is shown in Supplementary Table 1).

the behavioural results, tests were conducted at different ages, between 9 and 22 weeks old (Supplementary Fig. 4A). At 9–10 weeks of age, *Shank3B*$^{-/-}$ mice did not show anxiety in the light-dark box test, as evidenced by the similar amount of time spent in the light compared to WT mice (Supplementary Fig. 4B; $p = 0.101$). At the age of 10–15 weeks, *Shank3B*$^{-/-}$ mice spent as much time as WT mice in the open arms of the elevated plus maze (Supplementary Fig. 4C; $p = 0.606$). Similarly, at 18–22 weeks of age, no significant difference was observed in time spent in the centre zone of the open field test between *Shank3B*$^{-/-}$ and WT mice (Supplementary Fig. 4D; $p = 0.630$).

The results indicate that the observed behavioural deficiencies in *Shank3B*$^{-/-}$ mice were not influenced by anxiety.

3.4. *Elevated mTORC1 signalling in Shank3B*$^{-/-}$ *mice was normalised by metformin*

We investigated whether mTORC1 and MAPK/ERK pathways, which are implicated in the FXS mouse model, were also increased in *Shank3B*$^{-/-}$ mice (Fig. 4A) (Choi et al., 2024).

Phosphorylated S6 ribosomal protein (p-S6) (S240/244), a downstream target of mTORC1, was elevated in both the hippocampus and prefrontal cortex by 1.37 ± 0.15-fold and 1.14 ± 0.05-fold, respectively, in *Shank3B*$^{-/-}$ mice (Fig. 4B; hippocampus: $p = 0.002$; Fig. 4C; prefrontal cortex: $p = 0.008$). p-ERK was only marginally increased by 1.12 ± 0.06-fold in the hippocampus and 1.22 ± 0.08-fold in the prefrontal cortex of *Shank3B*$^{-/-}$ mice compared to WT mice (Fig. 4D; hippocampus: $p = 0.024$; Fig. 4E; prefrontal cortex: $p = 0.012$). p-S6 (S235/236), a downstream target of the MAPK/ERK pathway, was 1.16 ± 0.07-fold increased only in the hippocampus of *Shank3B*$^{-/-}$ mice (Fig. 4F; hippocampus: $p = 0.034$; Fig. 4G; prefrontal cortex: genotype main effect: $p = 0.642$). The marginal increase in ERK phosphorylation might explain the lack of hyperphosphorylation of eIF4E, a downstream target of the MAPK/ERK pathway (Fig. 4H; hippocampus: genotype main effect: $p = 0.569$; Fig. 4I; prefrontal cortex: genotype main effect: $p = 0.434$), unlike what was reported before in the FXS mouse model (Choi et al., 2024; Gantois et al., 2017). However, total protein levels of eIF4E were elevated by 1.25 ± 0.09-fold in both areas (Fig. 4H; hippocampus: $p = 0.020$; Fig. 4I; prefrontal cortex: $p = 0.042$), but total mRNA levels remained unchanged compared to WT mice (Supplementary Fig. 5A; hippocampus: $p = 0.103$; Supplementary Fig. 5B; prefrontal cortex: $p = 0.310$). The mechanism behind the increased eIF4E protein level is not immediately clear.

In the striatum (Supplementary Fig. 6A), neither p-S6 (S240/244) (Supplementary Fig. 6B; genotype main effect: $p = 0.455$) nor p-ERK

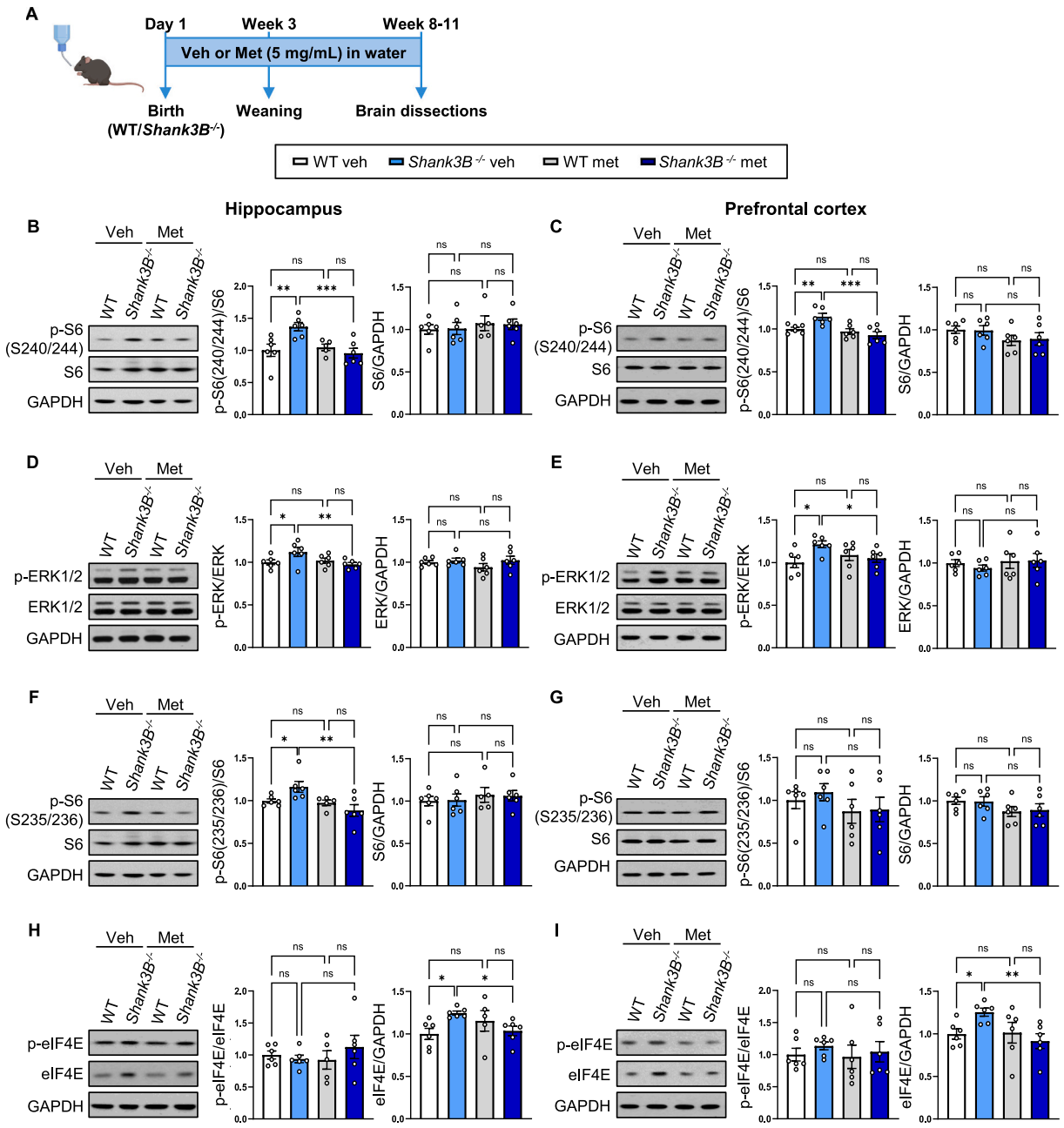

Fig. 4. Upregulated mTORC1 and minimally increased MAPK/ERK signalling pathways in the hippocampus and prefrontal cortex of *Shank3B*$^{-/-}$ mice were reduced with metformin treatment. (A) Brain structures were isolated at 8–11 weeks old after treatment from birth. Representative immunoblots from vehicle (veh) and metformin (met)-treated WT and *Shank3B*$^{-/-}$ mice of phosphorylated and total levels of (B—C, F-G) S6, (D-E) ERK, and (H—I) eIF4E in the hippocampus and prefrontal cortex. GAPDH was used as loading control. Protein levels were normalised to 1 for the WT veh, with other groups adjusted accordingly. Each point represents data from an individual mouse ($n = 5$–6), and all values (B—I) are shown as mean ± SEM, ***$p < 0.001$, **$p < 0.01$, *$p < 0.05$, ns = not significant versus all other groups; calculated by two-way ANOVA with Bonferroni's post hoc test (statistical analysis is shown in Supplementary Table 1).

(Supplementary Fig. 6C; genotype main effect: $p = 0.126$) levels were elevated in *Shank3B*$^{-/-}$ compared to WT mice.

Metformin normalised the enhanced mTORC1 signalling in the hippocampus and prefrontal cortex of *Shank3B*$^{-/-}$ to WT levels (Fig. 4B, C) (hippocampus: p-S6 (S240/244): $p < 0.001$; prefrontal cortex: p-S6 (S240/244): $p < 0.001$). The small increase in the MAPK/ERK signalling was also corrected, including p-S6 (S235/236) and total eIF4E (Fig. 4D-F, H-I; hippocampus: p-ERK: $p = 0.009$; p-S6 (S235/236): $p = 0.001$; eIF4E: $p = 0.043$; prefrontal cortex: p-ERK: $p = 0.047$; eIF4E: $p = 0.009$).

Thus, elevated mTORC1 signalling in the hippocampus and prefrontal cortex of *Shank3B*$^{-/-}$ mice was corrected by metformin.

3.5. Decreased GluN2B, Homer1, and GluA2 levels in *Shank3B*$^{-/-}$ mice were corrected by metformin

Since mTORC1 and MAPK/ERK pathways were not altered in the striatum, we studied GluN2B (also known as NR2B; an NMDAR subunit), Homer1b/c, and GluA2 (also known as GluR2; an AMPAR subunit), which are found in excitatory postsynapses associated with both these pathways, and were shown to be decreased in *Shank3B*$^{-/-}$ mice (Peça et al., 2011; Wang et al., 2024).

We measured GluN2B, Homer1, and GluA2 protein levels in the synaptosome fractioning of the striatum of WT and *Shank3B*$^{-/-}$ mice (Fig. 5A). As expected, *Shank3B*$^{-/-}$ mice showed a marked reduction in

these synaptic proteins: GluN2B was decreased by 43.2 ± 8.2 %, Homer1 by 32.6 ± 8.2 %, and GluA2 by 35.5 ± 7.2 % (Fig. 5B-D; $p < 0.001$). Metformin treatment significantly increased these proteins in *Shank3B*$^{-/-}$ mice, GluN2B by 1.39 ± 0.15-fold, Homer1 by 1.27 ± 0.12-fold, and GluA2 by 1.23 ± 0.12-fold (Fig. 5B-D; GluN2B: $p = 0.026$; Homer1: $p = 0.041$; GluA2: $p = 0.037$). However, GluA2 levels did not differ in the total striatal homogenate between genotypes or after treatment (Supplementary Fig. 6D; genotype main effect: $p = 0.485$; treatment main effect: $p = 0.322$).

4. Discussion

This study demonstrates that deletion of *Shank3* in mice leads to autistic-like behaviours, impaired learning and memory, and hyperactivation of the mTORC1 signalling pathway. Metformin treatment from birth corrected the behavioural deficits associated with ASD, restored hippocampal-dependent memory performance, reduced exaggerated signalling of the mTORC1 pathway, and corrected the decreased striatal synaptosomal proteins in *Shank3B*$^{-/-}$ mice.

We studied three core autistic-like behaviours in the *Shank3B*$^{-/-}$ mouse model: repetitive behaviour, social interaction, and communication. We confirmed earlier findings that *Shank3B*$^{-/-}$ mice presented increased self-grooming and a social preference impairment with no difference in social novelty in the three-chamber test (Dhamne et al., 2017; Kabitzke et al., 2018; Mei et al., 2016; Peça et al., 2011; Sgritta et al., 2019; Wang et al., 2017). We observed a decrease in USV frequency, in agreement with Pagani et al., and provided novel results of a reduction in USV duration, emphasising socio-communicative impairments (Burdeus-Olavarrieta et al., 2023; Pagani et al., 2019; Sarasua et al., 2014; Yao et al., 2023).

Metformin corrected FXS-like associated deficits: grooming, social interaction, and USVs, when mice were treated either at adult age or from birth (Choi et al., 2024; Gantois et al., 2017). Case reports documented the benefits of metformin in improving speech, social interaction, stereotypy, and cognition in adults and children with FXS (Biag et al., 2019; Dy et al., 2018). Here, we report that metformin administration from birth rescued repetitive behaviour, social preference, and USV duration, and partially improved USV frequency in *Shank3B*$^{-/-}$ mice.

Using the NOL test, we demonstrated impaired long-term hippocampal-dependent memory in *Shank3B*$^{-/-}$ mice. In contrast, they presented no impairment in long-term memory NOR, consistent with a prior study that used a short-term memory protocol for this test (Dhamne et al., 2017).

The contrasting results obtained in the NOL versus the NOR tests could be attributed to the engagement of different brain regions responsible for these tasks (Haettig et al., 2011; Vogel-Ciernia and Wood, 2014). The NOL test primarily relies on the hippocampus, which encodes for spatial information about the object, whereas the NOR test engages multiple brain areas, including the insular, ventromedial prefrontal and perirhinal cortex, and hippocampus, which are involved in processing the characteristics and features of the object (Haettig et al.,

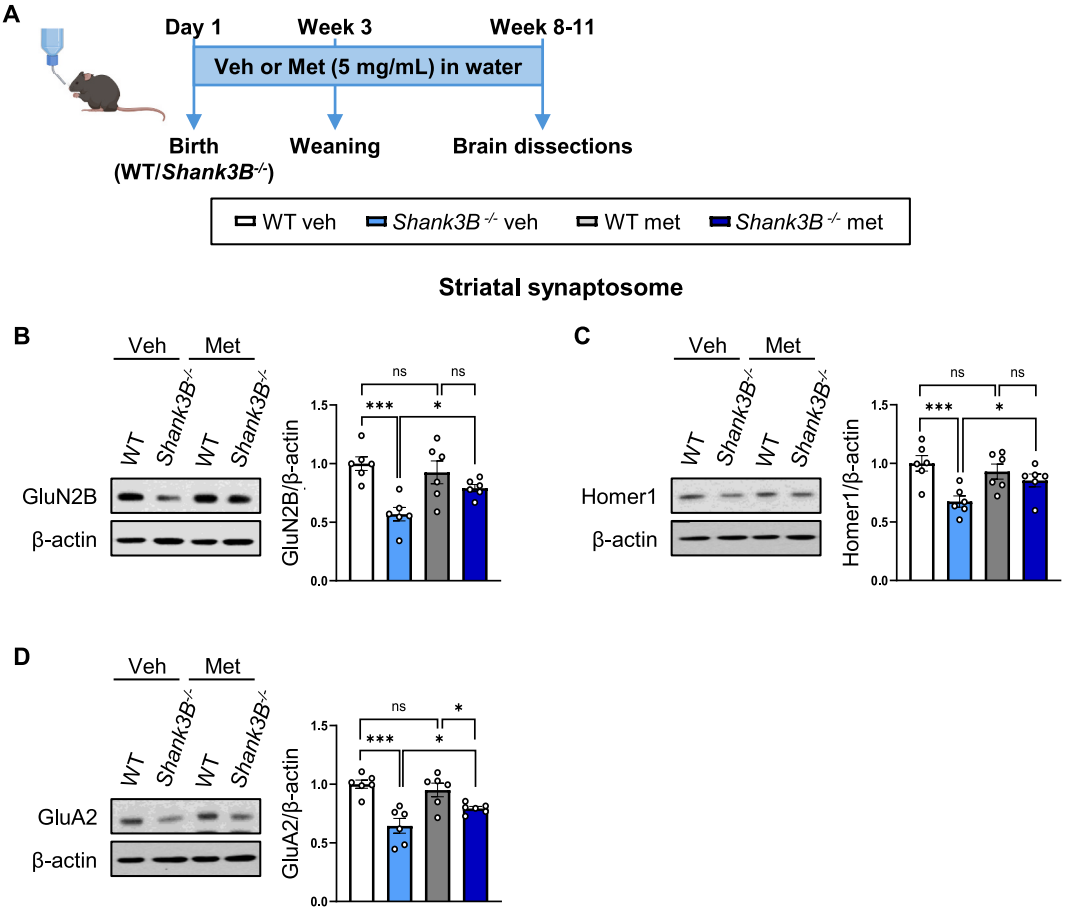

Fig. 5. Decreased GluN2B, Homer1 and GluA2 expression in striatal synaptosomes of *Shank3B*$^{-/-}$ mice was elevated by metformin treatment. (A) The striatum was isolated at 8–11 weeks old after treatment from birth. Representative immunoblots from vehicle (veh) and metformin (met)-treated WT and *Shank3B*$^{-/-}$ mice of total levels of (B) GluN2B, (C) Homer1, and (D) GluA2 in synaptosomes of the striatum. β-actin was used as loading control. Protein levels were normalised to 1 for the WT veh, with other groups adjusted accordingly. Each point represents data from an individual mouse ($n = 6$), and all values (B—D) are shown as mean ± SEM, ***$p < 0.001$, *$p < 0.05$, ns = not significant versus all other groups; calculated by two-way ANOVA with Bonferroni's post hoc test (statistical analysis is shown in Supplementary Table 1).

2011; Vogel-Ciernia and Wood, 2014).

mGluR-LTD plays an important role in learning and memory, and its dysregulation is evident in ASD mouse models, such as the FXS mouse (Collingridge et al., 2010; Ebert and Greenberg, 2013; Gantois et al., 2017). Although *Shank3B*$^{-/-}$ mice show disrupted striatal plasticity (Peça et al., 2011; Wang et al., 2017), including impaired DHPG-induced LTD in striatal D2 MSNs (Wang et al., 2017), multiple *Shank3* KO lines reported no change in hippocampal mGluR-LTD (Jaramillo et al., 2017; Kouser et al., 2013; Vicidomini et al., 2017). This lack of hippocampal alteration is consistent with our current findings. The brain region-specific dissociation suggests that the memory phenotype is not hippocampal mGluR-LTD dependent. NMDAR-dependent LTP and LTD are widely viewed as cellular mechanisms underlying learning and memory (Dupuis et al., 2023; Lüscher and Malenka, 2012). In several *Shank3* lines, hippocampal NMDAR-dependent LTP was reduced (Jaramillo et al., 2017; Kouser et al., 2013), whereas, as reported by Peça et al., paired-pulse ratio (PPR) and miniature excitatory postsynaptic currents (mEPSC) amplitude in CA1 were unchanged (Peça et al., 2011). Thus, LTP alterations could underline the hippocampal-dependent memory impairment we observed. However, direct measurement of hippocampal NMDAR-dependent LTP in *Shank3B*$^{-/-}$ mice is needed to test this hypothesis.

Metformin improved short-term and long-term memory in a FXS fly model and in a valproic acid-induced rat model of ASD, enhancing spatial memory in the Morris water maze test (Ishola et al., 2020; Monyak et al., 2017). In the NOL test, metformin treatment from birth corrected the reduced interaction with the object in the novel location to WT levels. However, metformin failed to ameliorate the hypomobility observed in *Shank3B*$^{-/-}$ mice, consistent with previous findings by Gantois et al. in which metformin did not rescue hyperactivity in the FXS mouse model (Gantois et al., 2017), indicating that metformin may have no effect on mobility.

Concerning anxiety, there is some controversy with certain studies reporting increased anxiety behaviours in *Shank3B*$^{-/-}$ mice (Peça et al., 2011; Szabó et al., 2025), while others observed no differences (Balaan et al., 2019; Dhamne et al., 2017; Szabó et al., 2025). Such discrepancies may be due to differences in the age of testing or handling practices. In our study, anxiety did not appear to influence the other behaviours, as no differences were detected between WT and *Shank3B*$^{-/-}$ mice in anxiety measures.

Shank3 deletion in the hippocampus and prefrontal cortex of *Shank3B*$^{-/-}$ mice resulted in increased activation of mTORC1 and minimal elevation of MAPK/ERK pathways. Previous studies showed elevated brain protein synthesis and mTORC1 activity in *Shank3* KO mice, and hyperactivation of the MAPK/ERK signalling pathway in *KRAS*-mutant cells with SHANK3 depletion (Lilja et al., 2024; Mencer et al., 2021; Torossian et al., 2021). Studies exploring the relationship between these pathways and SHANK3 are scarce, with inconsistent results among *Shank3* models, including *Shank3*-deficient neurons, PMS patient-derived neurons, and other *Shank3* transgenic mouse models (Bidinosti et al., 2016; Giona et al., 2025; Lee et al., 2017; Mencer et al., 2021; Moutin et al., 2021; Torossian et al., 2021).

We demonstrated that metformin treatment fully rescued the elevated signalling of the mTORC1 pathway. This finding is similar to our previous studies in a FXS mouse model, in which metformin administration from birth led to a reduction in mTORC1 and MAPK/ERK pathways activity, while treatment of adult mice (8–12 weeks) corrected exaggerated signalling only via the MAPK/ERK pathway (Choi et al., 2024; Gantois et al., 2017). In *Shank3B*$^{-/-}$ mice, mTORC1 is the primary dysregulated signalling cascade. Consistent with our findings, metformin has also been shown to inhibit the activation of the double-stranded RNA-dependent protein kinase (PKR), a key regulator of translation initiation, improving behavioural and neuropathological features in an amyotrophic lateral sclerosis and frontotemporal degeneration (ALS/FTD) mouse model (Zu et al., 2020).

We observed an increase in total eIF4E levels in the hippocampus and prefrontal cortex of *Shank3B*$^{-/-}$ mice, which was not reported before, and was corrected by metformin. Since eIF4E mediates cap-dependent translation (Pelletier et al., 2021), its upregulation could contribute to the exaggerated protein synthesis previously reported (Torossian et al., 2021). Since the *Eif4e* mRNA levels in *Shank3B*$^{-/-}$ mice did not differ from those of WT mice, the increased protein amount could occur at the translational or protein stability level. Future studies are needed to determine the underlying mechanistic basis.

Strikingly, there was neither an increase in mTORC1 nor in MAPK/ERK signalling in the striatum of *Shank3B*$^{-/-}$ mice. This could be explained by the presence of two distinct populations of striatal neurons, direct pathway spiny projection neurons (dSPNs) and indirect pathway SPNs (iSPNs) (Gerfen and Surmeier, 2011). Wang et al. demonstrated that in the striatum of male *Shank3B*$^{-/-}$ mice, only the iSPNs showed alterations in their spines and synaptic function (Wang et al., 2024). Another study linked grooming, a known impaired behaviour in *Shank3B*$^{-/-}$ mice, to hyperactivity of the iSPNs but not the dSPNs (Piantadosi et al., 2024). Western blotting analysis cannot detect cell-type-specific expression; therefore, further studies are necessary to analyse mTORC1 and MAPK/ERK signalling pathways in iSPNs and dSPNs.

Wang et al. reported that GluN2B levels were selectively decreased in the iSPNs of *Shank3B*$^{-/-}$ mice (Wang et al., 2024). Additionally, an earlier study showed that GluN2B protein expression was reduced in purified PSDs from the striatum of *Shank3B*$^{-/-}$ mice compared to WT (Peça et al., 2011). Moreover, Lopatynska-Mazurek et al. demonstrated that pre-treatment with rapamycin, an mTORC1 inhibitor, normalised the alcohol-induced changes in synaptosomal GluN2B levels in a rat model, reversing both increases and decreases (Lopatynska-Mazurek et al., 2021). This prompted us to investigate whether metformin could restore synaptosomal GluN2B expression in the striatum. We found that metformin treatment increased GluN2B levels in the striatum of *Shank3B*$^{-/-}$ mice.

As with GluN2B, Homer1 was also reduced in both iSPNs and the synaptosomal fraction of the whole striatum (Peça et al., 2011; Wang et al., 2024). Homer1 acts as a synaptic-associated protein linking Shank3 to mGluR (Sheng and Kim, 2000) (Fig. 1) and is consistently reduced across multiple *Shank3*-deficient mouse models (Bey et al., 2018; Mei et al., 2016; Peça et al., 2011). Since mGluR signal is crucial for LTD (Lüscher and Huber, 2010), Wang et al. reported impaired long-term synaptic plasticity preferentially in the iSPNs of *Shank3B*$^{-/-}$ compared to WT mice (Wang et al., 2017). This deficit led to excessive self-grooming in this mouse model, which was corrected by modulating iSPNs. Metformin corrected the reduced synaptosomal Homer1 expression in the striatum.

In contrast, GluA2 was decreased in both striatal populations of iSPNs and dSPNs, and, therefore, also in the synaptosomal fraction of the whole striatum (Peça et al., 2011; Wang et al., 2024). Salpietro et al. identified a neurodevelopmental disorder spectrum associated with *GRIA2* (the gene encoding for GluA2) de novo variants, including ASD (Salpietro et al., 2019). In accordance with previous research (Peça et al., 2011; Wang et al., 2024), we found a reduction in the synaptosomal expression of GluA2 in the striatum, which was reversed by metformin. Compartment-specific regulation of GluA2 was described in other contexts involving altered mTORC1 signalling. Pereyra et al. demonstrated that inhibition of mTORC1 in Wistar rats by rapamycin increased GluA2 levels in the hippocampal postsynaptic density, but not in the total homogenate. They hypothesised that this selective increase could be due to mTORC1-dependent effects on AMPAR local synthesis or trafficking, or from compensatory mechanisms secondary to reduced GluA1 levels (Pereyra et al., 2021). Consistent with this compartment-specific pattern, we also observed that metformin increased GluA2 levels only in the striatal synaptosome, while GluA2 levels in the total homogenate remained unchanged.

We chose to start metformin treatment early in life rather than in adulthood based on results from the FXS mouse model and clinical case

studies in FXS patients that demonstrate a better outcome in younger individuals (Biag et al., 2019; Choi et al., 2024; Dy et al., 2018). Early developmental periods appear to be sensitive to interventions targeting translational control pathways, such as p-S6, which is elevated during embryonic and early postnatal stages and gradually declines thereafter (Kouloulia et al., 2019). This may explain why metformin treatment initiated at birth normalised mTORC1 pathway levels in *Shank3B*$^{-/-}$ mice. The early-life approach limits direct conclusions about the therapeutic window relevant for older PMS patients. Also, since metformin influences systemic metabolism, peripheral changes could contribute to the central outcomes we observed. Future studies could distinguish peripheral metabolic modulation from direct central mechanisms, and administering metformin at different time points in life, such as after weaning (3 weeks old) or at adulthood, would be valuable for translating findings to the clinical population.

In conclusion, the findings of autistic-like behavioural impairments and cognitive deficits in *Shank3B*$^{-/-}$ mice recapitulate the phenotype observed in individuals with PMS. We report the underlying mechanism causing the behavioural deficits: elevated signalling of mTORC1 in the hippocampus and prefrontal cortex, and decreased levels of the receptor subunits GluN2B and GluA2, and the synaptic-associated protein Homer1 in the striatum. Importantly, metformin, an FDA-approved drug, corrected this aberrant signalling, resulting in improved behaviour. Given its safety, ready availability, and easy administration, metformin offers a promising therapeutic opportunity for rapid clinical translation to treat young male individuals with PMS.

CRediT authorship contribution statement

Laura Marsal-García: Writing – review & editing, Writing – original draft, Visualization, Software, Project administration, Methodology, Investigation, Formal analysis, Data curation, Conceptualization. **Jung-Hyun Choi:** Writing – review & editing, Project administration, Methodology, Investigation, Data curation, Conceptualization. **Eve Peraldi:** Writing – review & editing, Investigation, Data curation. **Pei You Wu:** Writing – review & editing, Investigation, Data curation. **Cong Loc Dang:** Writing – review & editing, Investigation, Data curation. **R. Anne McKinney:** Writing – review & editing, Supervision. **Ilse Gantois:** Writing – review & editing, Writing – original draft, Supervision, Project administration, Methodology, Investigation, Data curation, Conceptualization. **Nahum Sonenberg:** Writing – review & editing, Supervision, Funding acquisition.

Funding

This work was supported by the Canadian Institutes of Health Research (CIHR) Foundation grant [FDN-148423], the Azrieli Foundation, and the Norman Zavalkoff Family Foundation to N.S.; and by Global - Learning & Academic Research Institution for Master's·PhD students, and Postdocs (LAMP) Program of the National Research Foundation of Korea (NRF) grant funded by the Ministry of Education [No. RS-2024-00445180] to J.-H.C.

Declaration of competing interest

The authors declare that they have no known competing financial interests or personal relationships that could have appeared to influence the work reported in this paper.

Acknowledgements

We thank Eileen Hu, JiaHao Zhang, and Raquel Suissa for their research assistance; Annie Sylvestre and Annik Lafrance for animal care; and Niaz Mahmood and Caleb Walters for comments on the manuscript. The graphical abstract and Fig. 1 were created in BioRender. Sonenberg, N. (2025) https://BioRender.com/czihmfv, and https://BioRender.com/s7h9woc, respectively.

Appendix A. Supplementary data

Supplementary data to this article can be found online at https://doi.org/10.1016/j.nbd.2025.107217.

Data availability

All data are available in the main text or the supplementary materials.

The computer code produced in this study is available in the following database: Self-made Python script to sort the USV data into USV duration and calls per minute: Zenodo (doi: https://doi.org/10.5281/zenodo.14537932). The latest version is available on GitHub (https://github.com/Laura3-13/usv-utils).

References

American Psychiatric Association, 2013. Neurodevelopmental Disorders. In: Diagnostic and Statistical Manual of Mental Disorders *(5th ed)*, A.P. Association. American Psychiatric Publishing, Arlington, VA, pp. 31–86.

Amiel, S.A., 2021. The consequences of hypoglycaemia. Diabetologia 64, 963–970. https://doi.org/10.1007/s00125-020-05366-3.

Anagnostou, E., et al., 2016. Metformin for treatment of overweight induced by atypical antipsychotic medication in young people with autism Spectrum disorder: a randomized clinical trial. JAMA Psychiatry 73, 928–937. https://doi.org/10.1001/jamapsychiatry.2016.1232.

Angelakos, C.C., et al., 2019. Home-cage hypoactivity in mouse genetic models of autism spectrum disorder. Neurobiol. Learn. Mem. 165, 107000. https://doi.org/10.1016/j.nlm.2019.02.010.

Arons, M.H., et al., 2012. Autism-associated mutations in ProSAP2/Shank3 impair synaptic transmission and Neurexin–Neuroligin-mediated Transsynaptic signaling. J. Neurosci. 32, 14966–14978. https://doi.org/10.1523/jneurosci.2215-12.2012.

Balaan, C., et al., 2019. Juvenile Shank3b deficient mice present with behavioral phenotype relevant to autism spectrum disorder. Behav. Brain Res. 356, 137–147. https://doi.org/10.1016/j.bbr.2018.08.005.

Balasco, L., et al., 2022. Abnormal whisker-dependent behaviors and altered Cortico-hippocampal connectivity in Shank3b−/− mice. Cereb. Cortex 32, 3042–3056. https://doi.org/10.1093/cercor/bhab399.

Bey, A.L., et al., 2018. Brain region-specific disruption of Shank3 in mice reveals a dissociation for cortical and striatal circuits in autism-related behaviors. Transl. Psychiatry 8, 94. https://doi.org/10.1038/s41398-018-0142-6.

Biag, H.M.B., et al., 2019. Metformin treatment in young children with fragile X syndrome. Mol. Genet. Genomic Med. 7, e956. https://doi.org/10.1002/mgg3.956.

Bidinosti, M., et al., 2016. CLK2 inhibition ameliorates autistic features associated with SHANK3 deficiency. Science 351, 1199–1203. https://doi.org/10.1126/science.aad5487.

Bluck, S., 2003. Autobiographical memory: exploring its functions in everyday life. Memory 11, 113–123. https://doi.org/10.1080/741938206.

Bozdagi, O., et al., 2013. Insulin-like growth factor-1 rescues synaptic and motor deficits in a mouse model of autism and developmental delay. Mol. Autism. 4, 9. https://doi.org/10.1186/2040-2392-4-9.

Burdeus-Olavarrieta, M., et al., 2023. Consensus recommendations on communication, language and speech in Phelan-McDermid syndrome. Eur. J. Med. Genet. 66, 104745. https://doi.org/10.1016/j.ejmg.2023.104745.

Cammarata-Scalisi, F., et al., 2022. Clinical and genetic aspects of Phelan–McDermid syndrome: an interdisciplinary approach to management. Genes 13, 504. https://doi.org/10.3390/genes13030504.

Choi, J.H., et al., 2024. Early metformin treatment: an effective approach for targeting fragile X syndrome pathophysiology. Proc. Natl. Acad. Sci. USA 121, e2407546121. https://doi.org/10.1073/pnas.2407546121.

Collingridge, G.L., et al., 2010. Long-term depression in the CNS. Nat. Rev. Neurosci. 11, 459–473. https://doi.org/10.1038/nrn2867.

Cope, E.C., et al., 2023. Activation of the CA2-ventral CA1 pathway reverses social discrimination dysfunction in Shank3B knockout mice. Nat. Commun. 14, 1750. https://doi.org/10.1038/s41467-023-37248-8.

Crawley, J.N., 2004. Designing mouse behavioral tasks relevant to autistic-like behaviors. Ment. Retard. Dev. Disabil. Res. Rev. 10, 248–258. https://doi.org/10.1002/mrdd.20039.

Delling, J.P., Boeckers, T.M., 2021. Comparison of SHANK3 deficiency in animal models: phenotypes, treatment strategies, and translational implications. J. Neurodev. Disord. 13, 55. https://doi.org/10.1186/s11689-021-09397-8.

Desaunay, P., et al., 2020. Memory in autism spectrum disorder: a meta-analysis of experimental studies. Psychol. Bull. 146, 377–410. https://doi.org/10.1037/BUL0000225.

Dhamne, S.C., et al., 2017. Replicable in vivo physiological and behavioral phenotypes of the Shank3B null mutant mouse model of autism. Mol. Autism. 8, 1–19. https://doi.org/10.1186/s13229-017-0142-z.

Dupuis, J.P., et al., 2023. NMDA receptor functions in health and disease: old actor, new dimensions. Neuron 111, 2312–2328. https://doi.org/10.1016/j.neuron.2023.05.002.
Durand, C.M., et al., 2012. SHANK3 mutations identified in autism lead to modification of dendritic spine morphology via an actin-dependent mechanism. Mol. Psychiatry 17, 71–84. https://doi.org/10.1038/mp.2011.57.
Dy, A.B.C., et al., 2018. Metformin as targeted treatment in fragile X syndrome. Clin. Genet. 93, 216–222. https://doi.org/10.1111/cge.13039.
Ebert, D.H., Greenberg, M.E., 2013. Activity-dependent neuronal signalling and autism spectrum disorder. Nature 493, 327–337. https://doi.org/10.1038/nature11860.
Ensembl, 2025. SHANK3 Human and Mouse Transcript Variants. Available at: https://useast.ensembl.org/Human/Search/Results?q=SHANK3;site=ensembl;facet_species=Human;page=1;facet_feature_type=Transcript;perpage=10 https://useast.ensembl.org/Mouse/Search/Results?q=Shank3;site=ensembl;facet_species=Mouse;page=1;perpage=10;facet_feature_type=Transcript [Accessed: October 03, 2025].
Ferhat, A.T., et al., 2016. Recording mouse ultrasonic vocalizations to evaluate social communication. J. Vis. Exp. https://doi.org/10.3791/53871.
Fischer, I., et al., 2024. Shank3 mutation impairs glutamate signaling and myelination in ASD mouse model and human iPSC-derived OPCs. Sci. Adv. 10, eadl4573. https://doi.org/10.1126/sciadv.adl4573.
Fontbonne, A., et al., 1996. The effect of metformin on the metabolic abnormalities associated with upper-body fat distribution. BIGPRO Study Group. Diabetes Care 19, 920–926. https://doi.org/10.2337/diacare.19.9.920.
Gallagher, S.M., et al., 2004. Extracellular signal-regulated protein kinase activation is required for metabotropic glutamate receptor-dependent long-term depression in hippocampal area CA1. J. Neurosci. 24, 4859–4864. https://doi.org/10.1523/jneurosci.5407-03.2004.
Gantois, I., et al., 2017. Metformin ameliorates core deficits in a mouse model of fragile X syndrome. Nat. Med. 23, 674–677. https://doi.org/10.1038/nm.4335.
Gantois, I., et al., 2019. Metformin for treatment of fragile X syndrome and other neurological disorders. Annu. Rev. Med. 70, 167–181. https://doi.org/10.1146/annurev-med-081117-041238.
Gerfen, C.R., Surmeier, D.J., 2011. Modulation of striatal projection systems by dopamine. Annu. Rev. Neurosci. 34, 441–466. https://doi.org/10.1146/annurev-neuro-061010-113641.
Giona, F., et al., 2025. Shank3 modulates Rpl3 expression and protein synthesis via mGlu5: implications for Phelan McDermid syndrome. Mol. Psychiatry 30, 3599–3614. https://doi.org/10.1038/s41380-025-02947-9.
Glueck, C.J., et al., 2001. Metformin reduces weight, centripetal obesity, insulin, leptin, and low-density lipoprotein cholesterol in nondiabetic, morbidly obese subjects with body mass index greater than 30. Metabolism 50, 856–861. https://doi.org/10.1053/meta.2001.24192.
Guillory, S.B., et al., 2021. Social visual attentional engagement and memory in Phelan-McDermid syndrome and autism spectrum disorder: a pilot eye tracking study. J. Neurodev. Disord. 13, 58. https://doi.org/10.1186/s11689-021-09400-2.
Haettig, J., et al., 2011. HDAC inhibition modulates hippocampus-dependent long-term memory for object location in a CBP-dependent manner. Learn. Mem. 18, 71–79. https://doi.org/10.1101/lm.1986911.
Hale, T., et al., 2002. Transfer of metformin into human milk. Diabetologia 45, 1509–1514. https://doi.org/10.1007/S00125-002-0939-X.
Huang, Z., et al., 2024. Strategies for assessing autistic-like behaviors in mice. J. Vis. Exp. https://doi.org/10.3791/66846.
Huang, Z., et al., 2025. Hippocampal inhibitory interneuron-specific DREADDs treatment alters mTORC1-4E-BP signaling and impairs memory formation. J. Neurochem. 169, e70048. https://doi.org/10.1111/jnc.70048.
Ishola, I.O., et al., 2020. Novel potential of metformin on valproic acid-induced autism spectrum disorder in rats: involvement of antioxidant defence system. Fundam. Clin. Pharmacol. 34, 650–661. https://doi.org/10.1111/fcp.12567.
Jaramillo, T.C., et al., 2016. Altered striatal synaptic function and abnormal behaviour in Shank3 Exon4-9 deletion mouse model of autism. Autism Res. 9, 350–375. https://doi.org/10.1002/AUR.1529.
Jaramillo, T.C., et al., 2017. Novel Shank3 mutant exhibits behaviors with face validity for autism and altered striatal and hippocampal function. Autism Res. 10, 42–65. https://doi.org/10.1002/aur.1664.
Jesse, S., et al., 2020. Severe white matter damage in SHANK3 deficiency: a human and translational study. Ann. Clin. Transl. Neurol. 7, 46–58. https://doi.org/10.1002/acn3.50959.
Kabitzke, P.A., et al., 2018. Comprehensive analysis of two Shank3 and the Cacna1c mouse models of autism spectrum disorder. Genes Brain Behav. 17, 4–22. https://doi.org/10.1111/gbb.12405.
Kalueff, A.V., et al., 2015. Neurobiology of rodent self-grooming and its value for translational neuroscience. Nat. Rev. Neurosci. 17, 45–59. https://doi.org/10.1038/nrn.2015.8.
Kazdoba, T.M., et al., 2016. Behavioral phenotypes of genetic mouse models of autism. Genes Brain Behav. 15, 7–26. https://doi.org/10.1111/gbb.12256.
Kolevzon, A., et al., 2022. Clinical trial of insulin-like growth factor-1 in Phelan-McDermid syndrome. Mol. Autism. 13, 17. https://doi.org/10.1186/s13229-022-00493-7.
Kouloulia, S., et al., 2019. Raptor-mediated proteasomal degradation of Deamidated 4E-BP2 regulates postnatal neuronal translation and NF-κB activity. Cell Rep. 29, 3620–3635.e3627. https://doi.org/10.1016/j.celrep.2019.11.023.
Kouser, M., et al., 2013. Loss of predominant Shank3 isoforms results in hippocampus-dependent impairments in behavior and synaptic transmission. J. Neurosci. 33, 18448–18468. https://doi.org/10.1523/JNEUROSCI.3017-13.2013.
Krapivinsky, G., et al., 2003. The NMDA receptor is coupled to the ERK pathway by a direct interaction between NR2B and RasGRF1. Neuron 40, 775–784. https://doi.org/10.1016/S0896-6273(03)00645-7.
Leblond, C.S., et al., 2014. Meta-analysis of SHANK mutations in autism Spectrum disorders: a gradient of severity in cognitive impairments. PLoS Genet. 10, e1004580. https://doi.org/10.1371/journal.pgen.1004580.
Lee, Y., et al., 2017. Striatal transcriptome and Interactome analysis of Shank3-overexpressing mice reveals the connectivity between Shank3 and mTORC1 signaling. Front. Mol. Neurosci. 10, 201. https://doi.org/10.3389/fnmol.2017.00201.
Leger, M., et al., 2013. Object recognition test in mice. Nat. Protoc. 8, 2531–2537. https://doi.org/10.1038/nprot.2013.155.
Lilja, J., et al., 2024. SHANK3 depletion leads to ERK signalling overdose and cell death in KRAS-mutant cancers. Nat. Commun. 15, 8002. https://doi.org/10.1038/s41467-024-52326-1.
Liu, H.Y., et al., 2021. Dissection of the relationship between anxiety and stereotyped self-grooming using the mutant autistic model, acute stress model and chronic pain model. Neurobiol. Stress 15, 100417. https://doi.org/10.1016/j.ynstr.2021.100417.
Lopatynska-Mazurek, M., et al., 2021. Rapamycin improves spatial learning deficits, vulnerability to alcohol addiction and altered expression of the GluN2B subunit of the NMDA receptor in adult rats exposed to ethanol during the neonatal period. Biomolecules 11, 650. https://doi.org/10.3390/biom11050650.
Lüscher, C., Huber, K.M., 2010. Group 1 mGluR-dependent synaptic long-term depression: mechanisms and implications for circuitry and disease. Neuron 65, 445–459. https://doi.org/10.1016/j.neuron.2010.01.016.
Lüscher, C., Malenka, R.C., 2012. NMDA receptor-dependent long-term potentiation and long-term depression (LTP/LTD). Cold Spring Harb. Perspect. Biol. 4. https://doi.org/10.1101/cshperspect.a005710.
Ma, Y., et al., 2025. Shank3 related oligodendrocyte alterations in autism are restored by Erk pathway inhibition. Mol. Psychiatry. https://doi.org/10.1038/s41380-025-03333-1.
Maenner, M.J., et al., 2023. Prevalence and characteristics of autism Spectrum disorder among children aged 8 years - autism and developmental disabilities monitoring network, 11 sites, United States, 2020. MMWR Surveill. Summ. 72, 1–14. https://doi.org/10.15585/mmwr.ss7202a1.
Malara, M., et al., 2022. SHANK3 deficiency leads to myelin defects in the central and peripheral nervous system. Cell. Mol. Life Sci. 79, 371. https://doi.org/10.1007/s00018-022-04400-4.
Marsal-García, L., 2024. Usv-utils (Version 1.1.0). https://doi.org/10.5281/zenodo.14537932.
McLean, A.C., et al., 2012. Performing vaginal lavage, crystal violet staining, and vaginal cytological evaluation for mouse estrous cycle staging identification. J. Vis. Exp. e4389. https://doi.org/10.3791/4389.
Mei, Y., et al., 2016. Adult restoration of Shank3 expression rescues selective autistic-like phenotypes. Nature 530, 481–484. https://doi.org/10.1038/nature16971.
Memmott, R.M., et al., 2010. Metformin Prevents Tobacco Carcinogen–Induced Lung Tumorigenesis. Cancer Prev. Res. 3, 1066–1076. https://doi.org/10.1158/1940-6207.Capr-10-0055.
Mencer, S., et al., 2021. Proteomics of autism and Alzheimer's mouse models reveal common alterations in mTOR signaling pathway. Transl. Psychiatry 11, 480. https://doi.org/10.1038/s41398-021-01578-2.
Mina, A.I., et al., 2018. CalR: a web-based analysis tool for indirect calorimetry experiments. Cell Metab. 28 (656–666), e651. https://doi.org/10.1016/j.cmet.2018.06.019.
Monteiro, P., Feng, G., 2017. SHANK proteins: roles at the synapse and in autism spectrum disorder. Nat. Rev. Neurosci. 18, 147–157. https://doi.org/10.1038/nrn.2016.183.
Monyak, R.E., et al., 2017. Insulin signaling misregulation underlies circadian and cognitive deficits in a Drosophila fragile X model. Mol. Psychiatry 22, 1140–1148. https://doi.org/10.1038/mp.2016.51.
Morrel, J., et al., 2023. Neural correlates and predictors of speech and language development in infants at elevated likelihood for autism: a systematic review. Front. Hum. Neurosci. 17, 1211676. https://doi.org/10.3389/fnhum.2023.1211676.
Moutin, E., et al., 2021. Restoring glutamate receptosome dynamics at synapses rescues autism-like deficits in Shank3-deficient mice. Mol. Psychiatry 26, 7596–7609. https://doi.org/10.1038/s41380-021-01230-x.
Pagani, M., et al., 2019. Deletion of autism risk gene Shank3 disrupts prefrontal connectivity. J. Neurosci. 39, 5299–5310. https://doi.org/10.1523/jneurosci.2529-18.2019.
Peça, J., et al., 2011. Shank3 mutant mice display autistic-like behaviours and striatal dysfunction. Nature 472, 437–442. https://doi.org/10.1038/nature09965.
Peixoto, R.T., et al., 2019. Abnormal striatal development underlies the early onset of behavioral deficits in Shank3B(−/−) mice. Cell Rep. 29 (2016–2027), e2014. https://doi.org/10.1016/j.celrep.2019.10.021.
Pelletier, J., et al., 2021. The multifaceted eukaryotic cap structure. WIREs RNA 12, e1636. https://doi.org/10.1002/wrna.1636.
Pereyra, M., et al., 2021. AMPA receptor expression requirement during long-term memory retrieval and its association with mTORC1 signaling. Mol. Neurobiol. 58, 1711–1722. https://doi.org/10.1007/s12035-020-02215-7.
Phelan, K., et al., 2022. Phelan-McDermid syndrome: a classification system after 30 years of experience. Orphanet J. Rare Dis. 17, 1–4. https://doi.org/10.1186/S13023-022-02180-5/METRICS.
Phelan-McDermid Syndrome Foundation, 2025. What is Phelan-McDermid Syndrome? Available at: https://pmsf.org/what-is-phelan-mcdermid-syndrome/ [Accessed: 24 January 2025].

Piantadosi, S.C., et al., 2024. Hyperactivity of indirect pathway-projecting spiny projection neurons promotes compulsive behavior. Nat. Commun. 15, 4434. https://doi.org/10.1038/s41467-024-48331-z.
Pourfridoni, M., et al., 2024. Beneficial effects of metformin treatment on memory impairment. Mol. Biol. Rep. 51, 640. https://doi.org/10.1007/s11033-024-09445-1.
Rein, B., et al., 2020. A standardized social preference protocol for measuring social deficits in mouse models of autism. Nat. Protoc. 15, 3464–3477. https://doi.org/10.1038/s41596-020-0382-9.
Sala, C., et al., 2015. Shank synaptic scaffold proteins: keys to understanding the pathogenesis of autism and other synaptic disorders. J. Neurochem. 135, 849–858. https://doi.org/10.1111/JNC.13232.
Salpietro, V., et al., 2019. AMPA receptor GluA2 subunit defects are a cause of neurodevelopmental disorders. Nat. Commun. 10, 3094. https://doi.org/10.1038/s41467-019-10910-w.
Santini, E., Klann, E., 2014. Reciprocal signaling between translational control pathways and synaptic proteins in autism spectrum disorders. Sci. Signal. 7. https://doi.org/10.1126/scisignal.2005832 re10-re10.
Sarasua, S.M., et al., 2014. Clinical and genomic evaluation of 201 patients with Phelan-McDermid syndrome. Hum. Genet. 133, 847–859. https://doi.org/10.1007/s00439-014-1423-7.
Sgritta, M., et al., 2019. Mechanisms underlying microbial-mediated changes in social behavior in mouse models of autism spectrum disorder. Neuron 101, 246–259.e246. https://doi.org/10.1016/j.neuron.2018.11.018.
Shcheglovitov, A., et al., 2013. SHANK3 and IGF1 restore synaptic deficits in neurons from 22q13 deletion syndrome patients. Nature 503, 267–271. https://doi.org/10.1038/nature12618.
Sheng, M., Kim, E., 2000. The Shank family of scaffold proteins. J. Cell Sci. 113, 1851–1856. https://doi.org/10.1242/jcs.113.11.1851.
Szabó, J., et al., 2025. Autism-like phenotype across the lifespan of Shank3B-mutant mice of both sexes. J. Neurodev. Disord. 17, 45. https://doi.org/10.1186/s11689-025-09635-3.
Torossian, A., et al., 2021. Increased rates of cerebral protein synthesis in Shank3 knockout mice: implications for a link between synaptic protein deficit and dysregulated protein synthesis in autism spectrum disorder/intellectual disability. Neurobiol. Dis. 148, 105213. https://doi.org/10.1016/j.nbd.2020.105213.
U.S. National Library of Medicine, 2025. A Trial of Metformin in Individuals with Fragile X Syndrome (Met). ClinicalTrials.gov. Available at: https://clinicaltrials.gov/study/NCT03862950.
Urrutia-Ruiz, C., et al., 2022. Deletion of the autism-associated protein SHANK3 abolishes structural synaptic plasticity after brain trauma. Int. J. Mol. Sci. 23, 6081. https://doi.org/10.3390/ijms23116081.
Vicidomini, C., et al., 2017. Pharmacological enhancement of mGlu5 receptors rescues behavioral deficits in SHANK3 knock-out mice. Mol. Psychiatry 22, 689–702. https://doi.org/10.1038/mp.2016.30.
Vogel-Ciernia, A., Wood, M.A., 2014. Examining object location and object recognition memory in mice. Curr. Protoc. Neurosci. 69. https://doi.org/10.1002/0471142301.ns0831s69, 8.31.31-38.31.17.
Wang, W., et al., 2017. Striatopallidal dysfunction underlies repetitive behavior in Shank3-deficient model of autism. J. Clin. Invest. 127, 1978–1990. https://doi.org/10.1172/JCI87997.
Wang, X., et al., 2014. Transcriptional and functional complexity of Shank3 provides a molecular framework to understand the phenotypic heterogeneity of SHANK3 causing autism and Shank3 mutant mice. Mol. Autism. 5, 1–14. https://doi.org/10.1186/2040-2392-5-30.
Wang, Y.-Z., et al., 2024. Neuron type-specific proteomics reveals distinct Shank3 proteoforms in iSPNs and dSPNs lead to striatal synaptopathy in Shank3B−/− mice. Mol. Psychiatry 29, 2372–2388. https://doi.org/10.1038/s41380-024-02493-w.
Wiebe, S., et al., 2020. The eIF4E homolog 4EHP (eIF4E2) regulates hippocampal long-term depression and impacts social behavior. Mol. Autism. 11, 92. https://doi.org/10.1186/s13229-020-00394-7.
Yao, K., et al., 2023. A review of ultrasonic vocalizations in mice and how they relate to human speech. J. Acoust. Soc. Am. 154, 650–660. https://doi.org/10.1121/10.0020544.
Yerevanian, A., Soukas, A.A., 2019. Metformin: mechanisms in human obesity and weight loss. Curr. Obes. Rep. 8, 156–164. https://doi.org/10.1007/s13679-019-00335-3.
Zu, T., et al., 2020. Metformin inhibits RAN translation through PKR pathway and mitigates disease in C9orf72 ALS/FTD mice. Proc. Natl. Acad. Sci. USA 117, 18591–18599. https://doi.org/10.1073/pnas.2005748117.
Zwanenburg, R.J., et al., 2016. Is there an effect of intranasal insulin on development and behaviour in Phelan-McDermid syndrome? A randomized, double-blind, placebo-controlled trial. Eur. J. Hum. Genet. 24, 1696–1701. https://doi.org/10.1038/ejhg.2016.109.